

## High level triggers for explosive mafic volcanism: Albano Maar, Italy



J.K. Cross <sup>a,\*</sup>, E.L. Tomlinson <sup>b</sup>, G. Giordano <sup>c</sup>, V.C. Smith <sup>d</sup>, A.A. De Benedetti <sup>c</sup>, J. Roberge <sup>e</sup>, C.J. Manning <sup>a</sup>, S. Wulf <sup>f</sup>, M.A. Menzies <sup>a</sup>

<sup>a</sup> Dept of Earth Sciences, Royal Holloway University of London, Egham TW20 0EX, UK

<sup>b</sup> Department of Geology, Trinity College Dublin, College Green, Dublin 2, Ireland

<sup>c</sup> Department of Sciences, Università di Roma TRE, L.go S. Murialdo 1, 00146 Roma, Italy

<sup>d</sup> Research Laboratory for Archaeology and the History of Art, University of Oxford, Dyson Perrins Building, South Parks Rd, Oxford OX1 3QY, UK

<sup>e</sup> Posgrado ESIA-Ticomán, Instituto Politécnico Nacional (IPN), ESIA-Ticomán, Av. Ticomán #600, Mexico, D.F., Mexico

<sup>f</sup> GFZ German Research Centre for Geosciences, Potsdam, Germany

### ARTICLE INFO

#### Article history:

Received 23 January 2013

Accepted 2 November 2013

Available online 12 December 2013

#### Keywords:

Glass chemistry

Foidite

Assimilation

Mixing

Fractional crystallisation and magma evolution

### ABSTRACT

Colli Albani is a quiescent caldera complex located within the Roman Magmatic Province (RMP), Italy. The recent Via dei Laghi phreatomagmatic eruptions led to the formation of nested maars. Albano Maar is the largest and has erupted seven times between ca 69–33 ka. The highly explosive nature of the Albano Maar eruptions is at odds with the predominant relatively mafic ( $\text{SiO}_2 = 48\text{--}52$  wt.%) foiditic ( $\text{K}_2\text{O} = 9$  wt.%) composition of the magma. The deposits have been previously interpreted as phreatomagmatic, however they contain large amounts (up to 30%vol) of deep seated xenoliths, skarns and all pre-volcanic subsurface units. All of the xenoliths have been excavated from depths of up to 6 km, rather than being limited to the depth at which magma and water interaction is likely to have occurred, suggesting an alternative trigger for eruption. High precision geochemical glass and mineral data of fresh juvenile (magmatic) clasts from the small volume explosive deposits indicate that the magmas have evolved along one of two evolutionary paths towards foidite or phonolite. The foiditic melts record ca. 50% mixing between the most primitive magma and Ca-rich melt, late stage prior to eruption. A major result of our study is finding that the generation of Ca-rich melts via assimilation of limestone, may provide storage for significant amounts of  $\text{CO}_2$  that can be released during a mixing event with silicate magma. Differences in melt evolution are inferred as having been controlled by variations in storage conditions: residence time and magma volume.

Crown Copyright © 2013 Published by Elsevier B.V. All rights reserved.

### 1. Introduction

The volcanic products of the Colli Albani Volcanic District, including the most recently erupted magmas from Albano Maar, are defined as alkali-rich and silica undersaturated (mainly  $>7$  wt.%  $\text{K}_2\text{O}$ ,  $<50$  wt.%  $\text{SiO}_2$ ; tephrites to tephri-phonolites and K-foidites; Boari et al., 2009; Conticelli et al., 2010; De Benedetti et al., 2008; Freda et al., 2006, 2011; Gaeta et al., 2006, 2011; Giordano et al., 2006; Marra et al., 2003; Palladino et al., 2001; Trigila et al., 1995). Foiditic compositions have been found elsewhere worldwide i.e. Mt Vulture in Italy (D'Orazio et al., 2007), and at Eifel, Germany and Ngorangoro, Tanzania (Molle and Swisher, 2011; Shaw and Woodland, 2012 and the references therein). These compositions are typically erupted during low volume, effusive activity, often associated with carbonatitic magmatism. In contrast, products of Albano Maar are highly-fragmented, reflecting intense explosive activity, usually related to phreatomagmatism (Giordano and CARG Team, 2010; Giordano et al., 2002 and the references therein).

The Colli Albani Volcanic District magmas, like those erupted elsewhere in the RMP, originate from a heterogeneous, metasomatised,

phlogopite-rich mantle under high  $\text{XCO}_2$  caused by the decarbonation of subducted pelagic sediments rich in carbonate (Boari et al., 2009; Chiarabba et al., 2010; Chiodini and Frondini, 2001; Conticelli et al., 2010). The most recent activity at Colli Albani ( $<355$  ka) is associated with small volume eruptions of magmas characterised by some degree of assimilation of Mesozoic carbonate in the shallow magma plumbing system (1–6 km in depth; Boari et al., 2009; Di Rocco et al., 2012). Experimental work suggests that carbonate enhances the fractionation of Ca-rich clinopyroxene and suppresses the crystallisation of plagioclase feldspar and phlogopite in parental phono-tephrite melts, this effect is enhanced at elevated carbonate concentrations and therefore melts may evolve along different pathways depending on the degree of carbonate assimilation (Freda et al., 2008; Gaeta et al., 2009; Iacono Marziano et al., 2007, 2008; Mollo et al., 2010; Trigila et al., 1995). Part of the aim of this study was to compare the different compositions produced under the specific experimental conditions, with the large natural glass geochemical dataset presented herein, and thus investigate the evolution of these magmas both within and between eruptions.

A long-standing question regarding maar-diatreme mafic volcanism, including kimberlite volcanism, is the relative importance of magmatic  $\text{CO}_2$  and  $\text{H}_2\text{O}$  and external  $\text{H}_2\text{O}$  in promoting the fragmentation and the explosivity of low viscosity magmas (Lorenz, 1986; Russell et al.,

\* Corresponding author.

E-mail address: [joanna.k.cross@googlegmail.com](mailto:joanna.k.cross@googlegmail.com) (J.K. Cross).

2012). However, while the shape of the glass shards can be used as evidence in support of magma–water interaction (Büttner et al., 1999; Pardo et al., 2009; Wohletz, 1986) and evidence for low emplacement temperatures (e.g. Porreca et al., 2008), the contribution of magmatic volatiles to explosivity of maar-diatremes is more difficult to assess, making it an area of significant scientific interest.

Here we present micron-scale major (WDS-EMPA) and trace (LA-ICP-MS) element glass data for juvenile volcanic clasts from the last four of the seven known eruptions of Albano Maar (Units IV–VII; Table 1). The resultant geochemical dataset provides a new and larger range of juvenile magma compositions erupted at Albano Maar that has been published previously (De Benedetti et al., 2008; Freda et al., 2006; Gaeta et al., 2011; Giaccio et al., 2009) and provides additional information on the geochemistry, and spatial and temporal variability of Albano Maar magmas. The glass data is used to further constrain the evolution of Albano Maar magmas and gain insight into: (1) the relative roles of fractionation and crustal contamination on Albano Maar magma compositions; and (2) influences on explosivity and dispersal of Albano Maar tephra.

## 2. Geological background

The Colli Albani Volcanic District is a complex, overlapping volcanic edifice (Fig. 1; Giordano and CARG Team, 2010; Giordano et al., 2006), which developed along the Tyrrhenian margin of Italy within an extensional regime during the middle to late Pleistocene and through the Holocene (Avanzinelli et al., 2008, 2009; Rosenbaum and Lister, 2004). The Colli Albani Volcanic District is located in a densely populated area south of Rome, therefore understanding of its volcanic history and potential hazard is of critical importance. It has been active since ca. 600 ka with the early formation of a large caldera complex due to the eruption of intermediate to large volume ignimbrites, followed by post-caldera activity (<355 ka), accompanied by a significant reduction of the average eruption rate over time (Giordano and CARG Team, 2010; Giordano et al., 2006). Albano Maar is the locus of the most recent activity at the Colli Albani Volcanic District and has erupted at least 7 times between ca. 69 ka and 33 ka (De Benedetti et al., 2008; Freda et al., 2006; Funicello et al., 2003; Gaeta et al., 2011; Giaccio et al., 2009; Giordano and CARG Team, 2010; Giordano et al., 2002, 2006; Marra

et al., 2003), forming a nested maar-diatreme complex. The maar-complex is aligned NNW–SSE and N–S, parallel to earlier effusive activity and linking it with the central Colli Albani Volcanic District (Anzidei et al., 2008; Boari et al., 2009; De Benedetti et al., 2008; Freda et al., 2006; Gaeta et al., 2011; Giordano et al., 2006). Until recently, the Colli Albani Volcanic District, was considered to be quiescent and incapable of further activity (De Rita et al., 1995; Karner et al., 2001). This view has recently been challenged on the basis of emerging young ages for these deposits (De Benedetti et al., 2008; Freda et al., 2006; Funicello et al., 2003), occurrence of frequent seismic swarms and ground deformation (Chiarabba et al., 1997), and ongoing CO<sub>2</sub> emission in the Albano area, as indicated by CO<sub>2</sub> oversaturated groundwater (Anzidei et al., 2008; Chiodini and Frondini, 2001). This CO<sub>2</sub> emission may have also been the cause of a series of Lake Albano overturns and lahars, some as young as ca. 5.8 ± 0.1 ka <sup>14</sup>C, whose deposits (Fig. 1) are referred to as the Tavolato formation (De Benedetti et al., 2008; Funicello et al., 2003).

Sedimentary xenoliths and seismic tomography indicate that the shallow crust below the Colli Albani Volcanic District consists of Mesozoic carbonate basement at a depth of 1–6 km, overlain by Pliocene sediments (reviewed in Chiarabba et al., 2010; Danese and Mattei, 2010). Modelling of seismic data indicate that remains of the solidified main magma reservoir are located below the carbonate basement of the volcano edifice (>6 km depth, Chiarabba et al., 2010 and the references therein). This is in agreement with petrologic data by Boari et al. (2009), which indicate that the early caldera history at Colli Albani (>355 ka) is associated with a main magma reservoir located below 6 km depth, with no evidence of interaction with the shallow carbonates. A shallowing of the plumbing system is instead evident for the post-caldera stage (<355 ka), when a series of smaller volume reservoirs interacted with the shallow carbonates (Boari et al., 2009; Di Rocco et al., 2012). Recent seismic unrest appears to be linked to inflation of a magma source in the central-western area beneath the Via Dei Laghi maars (Anzidei et al., 2008; Chiarabba et al., 1997 and the references therein). 3D wave velocity models suggest it may be due to new magma accumulating (Bianchi et al., 2008; Chiarabba et al., 1997, 2010). This influx of new magma into the carbonate basement and resulting decarbonation reactions could be the cause of the current large CO<sub>2</sub> out fluxes (Carapezza and Tarchini, 2007; Chiodini and Frondini, 2001) and points towards potential hazard created by this volcano in the future.

**Table 1**  
Proximal and distal sample descriptions.

Sample	Unit	Clast type	Age (ka)	Location/depth of tephra	% ves <sup>#</sup>	% cryst <sup>#</sup>	Modal percentages of main phases of clasts/shards <sup>*</sup>	Modal percentages of unit components <sup>α</sup>	Emplacement mechanisms
10AH07Sc1	VII	Proximal pumice	33 ± 4 <sup>*</sup>	Within the surge	40	60	lc: 70%; gl: 21%; cpx: 7%; ap: 2%	JC: 90%; L: 2%; EP: 4%; Met. C: 2%; MC + MI: 2%	Fall and flow
AH07B	50 cm above?			25	80	gl: 38%; lc: 31%; cpx: 28%; mt: 3%			
AH07A	Base of unit within 15 cm of a/the thick pumice rich layer			35	76	gl: 45.5%; 35.5% lc; x: 10%; bi: 8.5%; cpx: 1%			
10AH062	VI	Magmatic intrusive	–	Basal breccia	40	75	lc: 41%; gl: 40%; cpx: 10%; x: 7%; mt: 1%; ap: 1%	JC: 80%; L: 2%; EP: 10% SC: 2%; Met. C: 2%; MC + MI: 4%	Base surge and ballistic fallout
AH05	V			Basal breccia	40–50	75	lc: 70%; gl: 20%; cpx: 8%; mt: 2%	JC: 1%; L: 60%; EP: 20% SC: 5%; Met. C: 9%; MC + MI: 5%	Pyroclastic density current
10AH042	IV	Magmatic intrusive	40 ± 6 <sup>*</sup>	1 m above base	30	80	san: 40%; phl: 20%; cpx: 15%; lc: 11%; gl: 10%; mt: 2%; ap: 2%	JC: 15%; L: 30%; EP: 5% SC: 20%; Met. C: 5%; MC + MI: 25%	Base surge and ballistic fallout
10AH041				Base	40	60	cpx: 48%; gl: 24%; lc: 14%; phl: 12%; mt: 2%		
TGOmis	I <sup>ε</sup>			Basal breccia	–	–	lc: 45%; cpx: 42%; ca: 6%; ap: 5%; gl: 2%	–	–
10AH05cum	V <sup>ε</sup>		36 ± 3–40 ± 6 <sup>*</sup>	Basal breccia	–	–	cpx: 75%; phl: 11%; lc: 7%; ca: 4%; ap: 2%; gl: 1%	–	

<sup>\*</sup>Gaeta et al. (2011) (<sup>39</sup>Ar/<sup>40</sup>Ar ages); <sup>\*</sup>Clinopyroxene (cpx), Phlogopite (phl), Leucite (lc), Sanidine (San), Kspar (kf), Biotite (bi), Apatite (ap), Magnetite (mt), Glass (gl), Calcite (ca); <sup>#</sup>Data collected by eye and point counting and is therefore subjective; <sup>α</sup>De Benedetti et al. (2010); abbreviations: Juvenile clasts (JC), lavas (L), sedimentary clasts (SC), magmatic cumulates and magmatic intrusives (MC + MI), metamorphosed clasts (Met. C), earlier pyroclastics (EP). <sup>ε</sup>Although the intrusive clasts are found in a specific unit, they have not been compared specifically to the glass from this unit as we cannot be confident as to their eruptive origin.

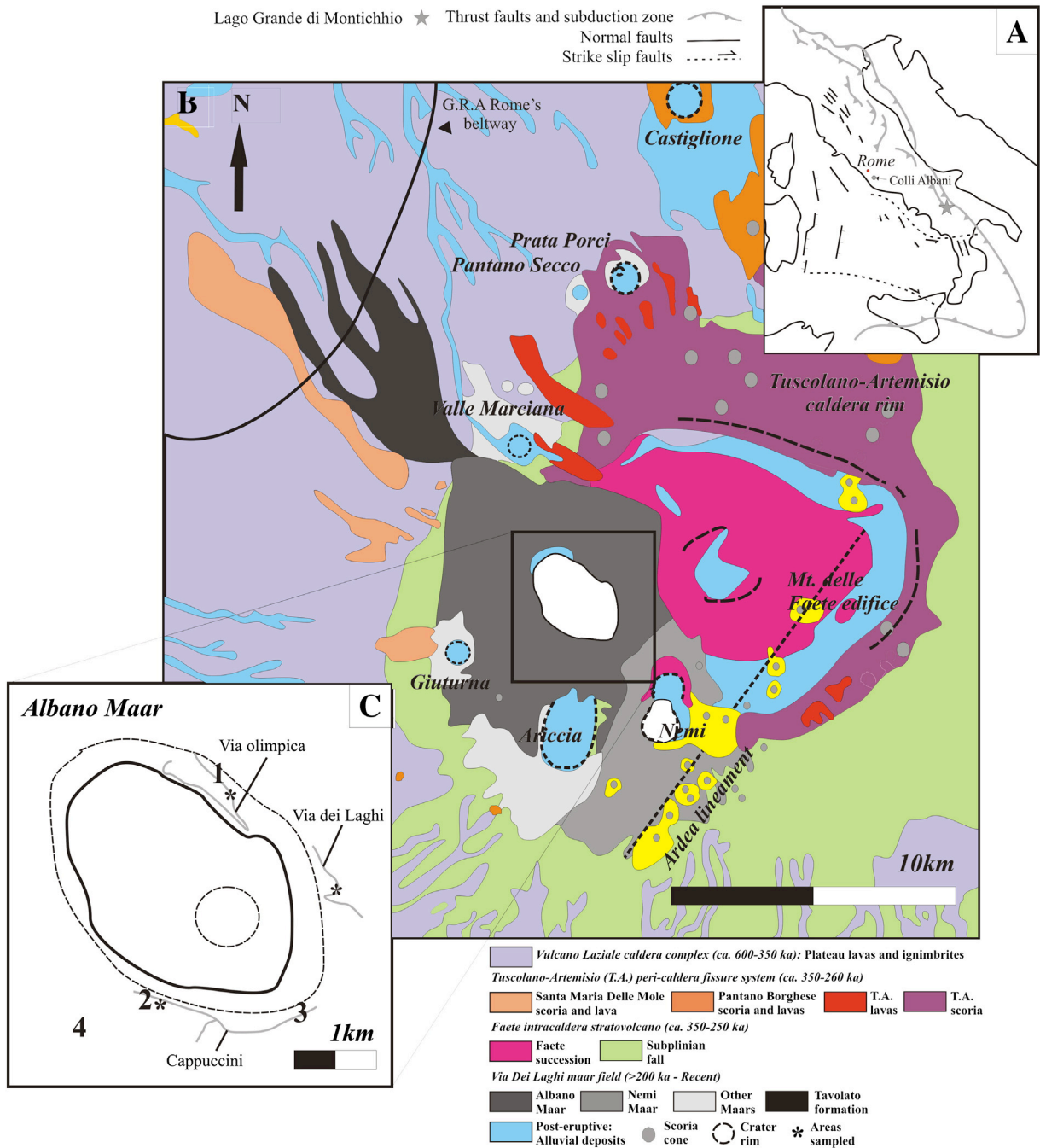


**Fig. 1.** (A) Schematic location map of Italy with tectonic regime and location of Colli Albani marked; (B) Simplified geological map of Colli Albani; (C) Albano Maar, sampling areas are marked, see Fig. 2 for stratigraphic columns (after De Benedetti et al., 2008).

### 3. Tephra deposits and samples

Albano Maar volcanic deposits form a succession of fine, ash-dominated base-surge, fall and flow deposits, associated with lithic-rich layers and breccia lenses (Figs. 1 and 2; Giordano and CARG Team, 2010; Giordano et al., 2002). The deposits contain large amounts of deep-seated xenoliths, which include intrusives, cumulates, skarns, thermometamorphic marbles and hornfels, and pre-volcanic sedimentary basement (De Benedetti et al., 2008, 2010). Fallout dispersal has been modelled to the east up to 120 km from the Albano Maar vent within several intermountain basins and associated with significant plumes (Giaccio et al., 2007; Sotilli et al., 2008). Samples from the uppermost units (IV–VII), the most recent of the seven recognised units in the youngest eruptive cycle, are considered to be representative of the range of eruptive

styles. Samples were collected from proximal outcrops where the volcano-stratigraphy is well exposed (sampling locations, Figs. 1 and 2).

#### 3.1. Juvenile clasts

Pumice clasts (0.3 to 0.5 cm in size) were held within a consolidated breccia or ash fall deposit and were extracted with a micro-drill or dremmel. Between 12 and 16 clasts were picked from each unit and their external rim was removed. Clasts were crushed to liberate glass shards from each sample, which were then mounted for analysis. In addition, large (10–30 cm in size) pumice ‘blocks’ were found within the flow and surge deposits.

The distal samples described and analysed in this study are described in the supplementary material.

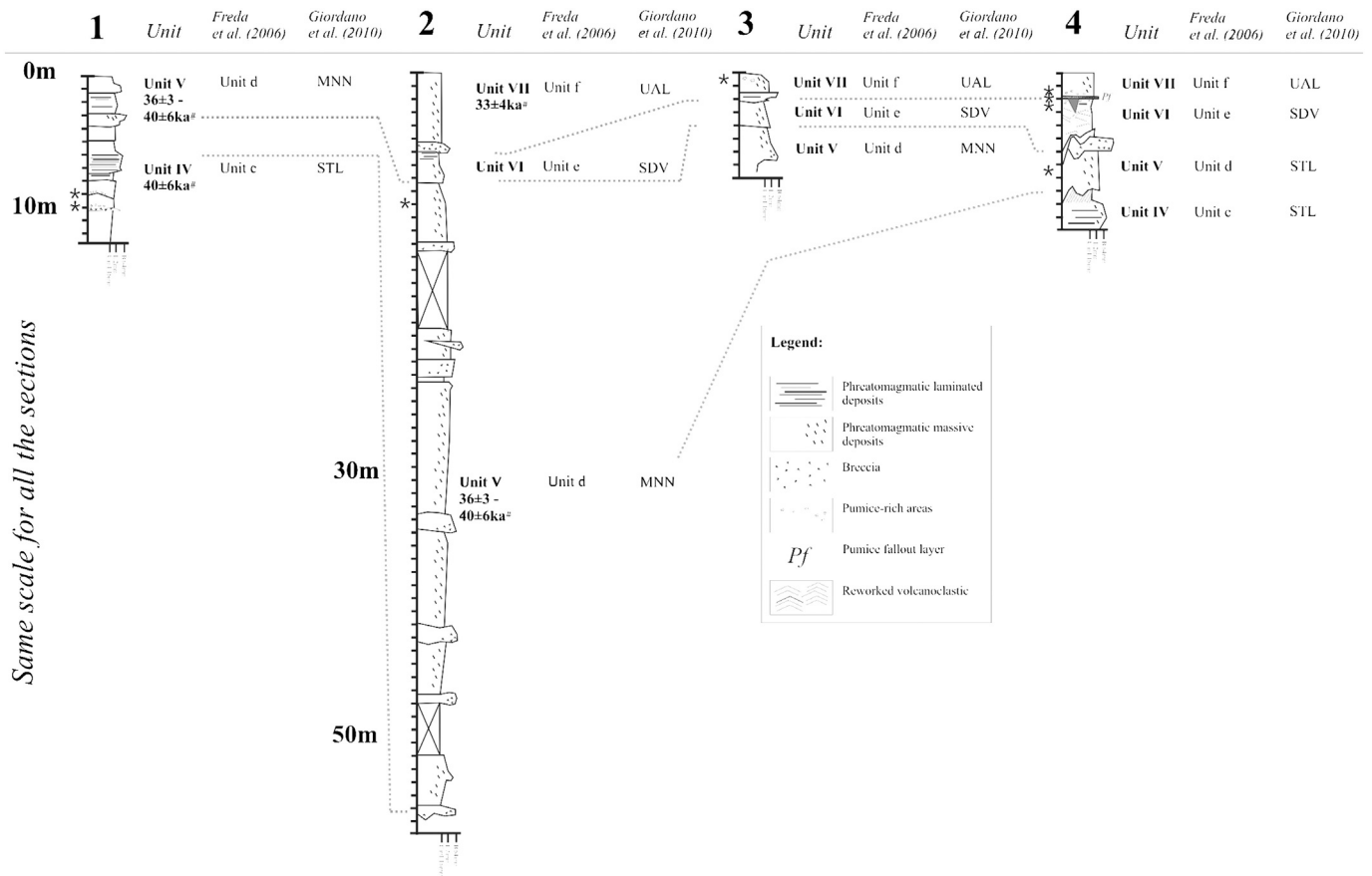


Fig. 2. Stratigraphic logs of locations in Fig. 1C. Symbol (\*) highlights the positions that were sampled.  $^{39}\text{Ar}/^{40}\text{Ar}$  ages from leucite crystals are marked, symbol (#) represents data from Gaeta et al. (2011). Previous nomenclature for the erupted units is listed (Freda et al., 2006; Giordano and CARG Team, 2010).

### 3.2. Magmatic intrusives

Intrusive clasts (10AH05cum and TGOmis) contain clinopyroxene, leucite, phlogopite, magnetite, apatite and calcite, and all crystals are subhedral in shape. The two clasts have different predominant grain sizes (200  $\mu\text{m}$ –2 cm; Fig. 4C and D) and different ratios of clinopyroxene to leucite along with minor differences in the abundances of other components (Table 1).

### 3.3. Sample preparation

Juvenile clasts and magmatic intrusives were sectioned and mounted so as to preserve their internal structure and texture (Fig. 3; details in Table 2). All samples were mounted in Struers EpoFix resin. Back-scattered Electron (BSE) images were taken using a desktop Scanning Electron Microscope (SEM; Hitachi TM-1000) in the Earth Sciences department, Durham University, UK and using the back-scatter detector attached to the JEOL 8600 wavelength dispersive electron microprobe (WDS-EPMA) at the Research Laboratory for Archaeology and the History of Art, University of Oxford, UK.

## 4. Analytical methods

### 4.1. WDS-EPMA

Major element compositions of the glasses were determined using the JEOL 8600 WDS-EPMA at the Research Laboratory for Archaeology and the History of Art, University of Oxford. A 15 kV, 4–6 nA, defocused beam was used (10  $\mu\text{m}$  was preferred but 5  $\mu\text{m}$  was used when sample was microlite-rich) to analyse glass. Phenocrysts and microcrysts were analysed using a 15 kV, 10–15 nA, focussed beam. The instrument

was calibrated with a suite of mineral standards and the accuracy and precision were assessed from analysis of MPI-DING reference glasses (Jochum et al., 2006), ATHO-G and StHs6/80-G and for the crystal analyses a range of Smithsonian standards were analysed as secondary standards (see supplementary data). The error values define precision at  $\pm 0.9\text{RSD}$  for  $\text{SiO}_2$  and  $\pm 8\text{RSD}$  for all other analysed elements with concentrations  $>0.15$  wt.%. Elements with concentrations  $<0.15$  wt.% typically have errors of  $\pm 40\text{RSD}$  and are not considered during data analysis. All analyses have accuracies of  $<5\%$  bias. Reported data are single spot analyses, averaging has been avoided so as to reflect the geochemical variation of glass between clasts of a single type. All of the data in graphs have been normalised to 100% (anhydrous) unless stated otherwise. Poor analyses, those with totals of  $<95\%$ , were discarded, in keeping with what is accepted by the European tephra community. Error bars on plots represent reproducibility, calculated as  $2\sigma$  of replicate analysis of MPI-DING StHs6/80-G (see supplementary data).

### 4.2. LA-ICP-MS

Trace elements were determined using Laser-Ablation Conductively-Induced-Plasma Mass Spectrometry (LA-ICP-MS), using an Agilent 7500ce coupled to a Resonetics 193 nm ArF excimer laser ablation system (RESOLUTION M-50 prototype) with a two-volume Laurin ablation cell at Royal Holloway, University of London (Müller et al., 2009). For glass analyses a 25–34  $\mu\text{m}$  laser beam diameter was used and completed at a repetition rate of 5 Hz. The ablation time used was 40 s on the sample, with 40 s of counting time of the gas blank (background), which was then subtracted from the sample signal to correct for polyatomic interferences. The analyses of the unknown sample were bracketed by analyses of the calibration standard NIST612. Analyses were

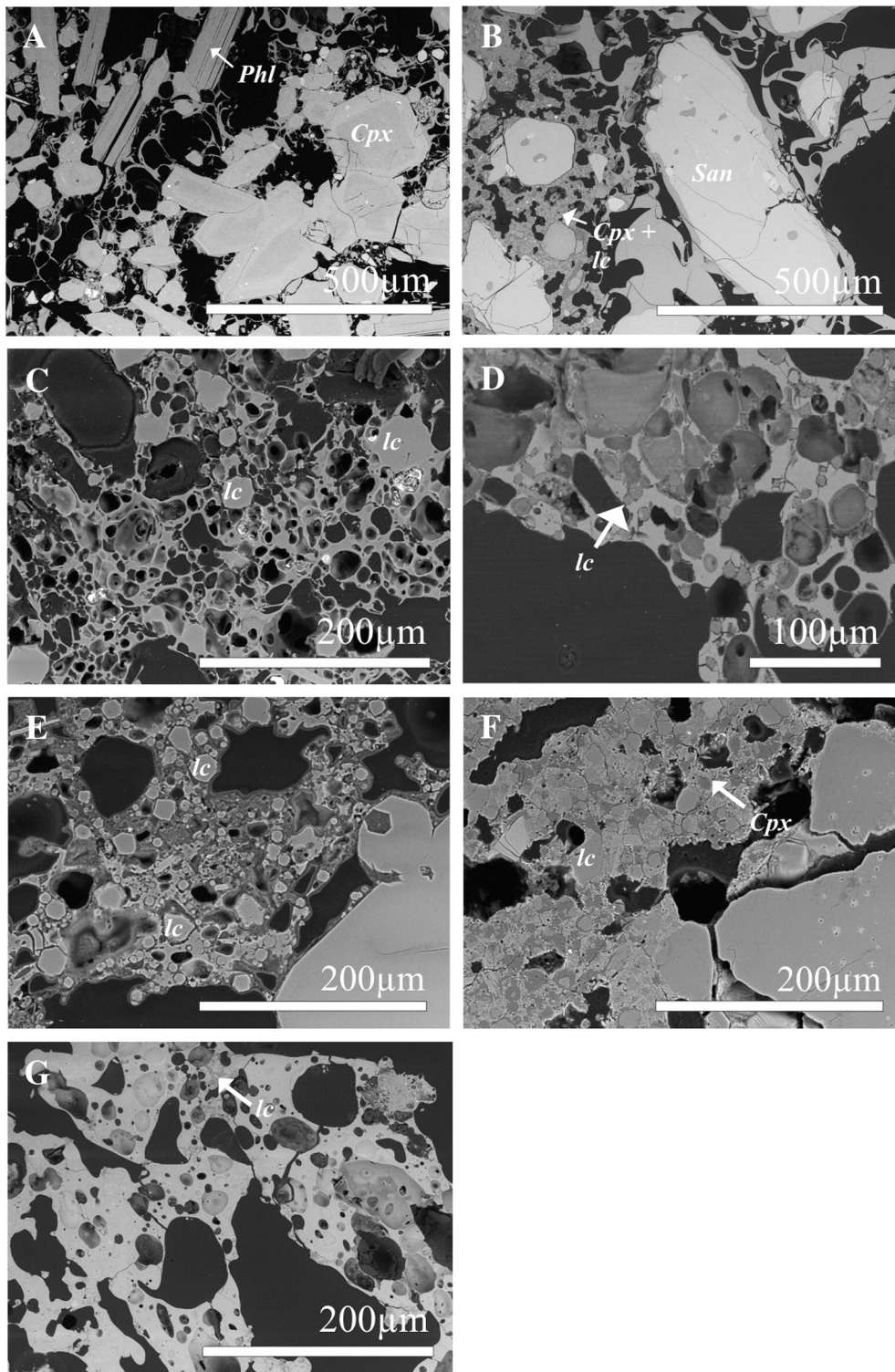


**Fig. 3.** SEM (BSE) images and a photograph of representative clasts from Units IV, V and VI. (A) Unit IV (10AH041), moderate to high vesicularity and high contents of euhedral clinopyroxene and leucite microcrysts. (B) Unit IV (10AH042), moderate to high vesicularity with a larger proportion of matrix glass and sanidine, clinopyroxene and phlogopite contents. (C) Unit V (AH05), highly vesicular clasts with matrix glass and very thin vesicle walls held together with leucite microcrysts. (D) Unit VI (10AH062), moderately vesiculated glass with small proportion of leucite microcrysts. (E) Unit VII (AH07A), moderately vesiculated with a large number of leucite microcrysts, some of which have affected the vesicle shapes. (F) Unit VII (AH07B), poorly to moderately vesiculated and heavily crystallised with leucite and clinopyroxene microcrysts. Unit VII (10AH07Sc1), moderate to high vesicularity with syn-eruptive crystallisation of leucite microcrysts.

then calibrated to  $^{29}\text{Si}$ , the values of which were taken from WDS-EPMA analyses of the same sample area prior to LA-ICP-MS analysis. For full details on data processing see Tomlinson et al. (2010). Each data point referred to in this study represents an individual spot analysis. The

external standard data acquired (MPI-DING glasses, i.e. ATHO-G and StHs6/80-G; Jochum et al., 2006; GEOREM, 11/2006) with a precision better than <10%RSD for the higher abundance elements (V, Rb, Sr, Y, Zr, Nb, Ba, La, Ce, Pr, Nd, Pb, Th, U) and <30%RSD for the others (Sm,

**Table 2**  
Major element analyses of proximal matrix glass (wt.%). Data displayed are examples of single spot analyses that reflect the geochemical variation witnessed within glass of a single clast type. Full dataset provided in supplementary data.

Sample	10AH041			10AH042			AH05		10AH062		AH07A		AH07B		10AH07Sc1			10AH05cum				
Unit	IV						V		VI		VII		Magmatic intrusive									
No. of analyses	38 (10 µm)			23 (10 µm)			11 (5 µm)		42 (10 µm)		6 (10 µm)		14 (10 µm)		33 (10 µm)			20 (µm)				
SiO <sub>2</sub>	48.99	49.3	50.28	58.4	58.36	57.06	49.13	48.9	49.66	48.9	49.6	51.86	47.94	49.46	48.66	52.7	51	49.64	50.24	0.04	0.02	0.7
TiO <sub>2</sub>	0.54	0.59	0.56	0.6	0.51	0.6	0.17	0.18	0.45	0.5	0.28	0.37	0.52	0.49	0.36	0.23	0.23	0.29	0.26	0.04	<LOD	<LOD
Al <sub>2</sub> O <sub>3</sub>	21.01	20.91	21.24	18.64	18.35	17.74	22.32	23	21.69	21.4	22.3	20.39	20.62	21.66	21.7	22.82	23.59	22.69	22.72	0.01	0.02	0.04
FeO <sub>(t)</sub>	5.29	6.08	4.64	4.19	3.89	4.5	4.04	3.84	4.52	4.62	3.1	2.91	5.72	4.8	4.8	3.47	3.39	3.92	3.51	0.04	0.14	0.03
MnO	0.03	0.16	0.12	0.02	0.1	0.11	0.42	0.49	0.23	0.16	0.14	0.07	0.1	0.11	0.25	0.18	0.27	0.23	0.28	<LOD	<LOD	<LOD
MgO	0.43	0.61	0.32	0.24	0.23	0.21	0.27	0.28	0.65	0.68	0.28	1.56	1.02	0.29	0.42	0.3	0.21	0.38	0.29	0.07	0.04	0.07
CaO	5.68	5.93	5.41	2.84	2.71	3.92	3.23	2.55	6.03	6.5	4.72	5.05	6.87	4.06	4.88	3.56	4.51	5.18	4.63	56.23	55.46	70.35
Na <sub>2</sub> O	3.57	4.11	3.7	5.12	5.12	5.98	9.25	10.05	5.63	7.11	7.01	0.97	3.52	3.39	4.82	2.67	7.18	7.9	8.04	0.07	<LOD	0.29
K <sub>2</sub> O	10.76	11.08	11.5	9.15	9.43	8.34	8.33	7.06	9.27	7.11	8.72	15.38	11.17	12.85	10.8	14.24	8.21	6.71	7.22	0.14	0.04	0.13
Total	96.3	98.77	97.77	99.2	98.7	98.46	97.16	96.35	98.13	96.98	96.15	98.56	97.48	97.11	96.7	100.17	98.59	96.94	97.19	56.64	55.72	71.61

Eu, Gd, Dy, Er, Yb, Lu, Ta). Relative standard error (RSE) on sample analysis is <2% for all elements. Error bars on plots represent reproducibility, calculated as a 2σ of replicate analysis of MPI-DING StHs6/80-G. Data have accuracies of typically <5% bias.

## 5. Results

### 5.1. Juvenile (pumice) clasts

The proximal juvenile clasts are crystal-rich (60–80% melt referenced, total crystallinity, Table 1), and dominated by microcrysts (35–50%). The clasts also contain a large proportion of xenocrystic and other lithic material (10–15%; Table 1). Crystal-rich clasts (50–60%) have lower vesicle percentages (<30%; Fig. 3E and F), while the other clasts (40% crystals) are more vesicular with equant vesicle shapes (40%; Fig. 3A, B, C, D and G). More than one pumice clast type is found within different layers of the stratigraphy of each erupted unit, each with a difference in crystallinity and vesicularity (Table 1).

The clasts fall into three groups, based on mineralogy:

*Clinopyroxene- and leucite-rich K-foidite* (up to 28% and <40% respectively). Also contain Fe–Ti oxides and apatite.

*Leucite-rich (70%) K-foidite*. Also contain Fe–Ti oxides and apatite.

*Sanidine-rich (40%) phonolite*. Also contain phlogopite, Ca-rich clinopyroxene and apatite.

We also recognise samples that are transitional between clinopyroxene- and leucite-rich and leucite-rich K-foidites.

#### 5.1.1. Clinopyroxene and leucite-rich K-foidites

The samples that fall into this group are 10AH041 (Unit IV), 10AH062 (Unit VI), AH07A and AH07B (Unit VII). The glasses are classed as foiditic (48–53 wt.% SiO<sub>2</sub>, 13–16 wt.% Total alkalis; Fig. 5). The matrix glass compositions span a wide range in both MgO (0.3–1.1 wt.%) and Na<sub>2</sub>O (2.5–8.0 wt.%; Fig. 6A). Glasses also show very high K<sub>2</sub>O contents (10.7–15.4 wt.%; Fig. 6B). The glass analyses in this group have a large range in CaO contents within a single clast type (Fig. 6C). This range in CaO contents is also evident in Fig. 4D and E with a linear positive trend with FeO<sub>t</sub> and a linear negative trend with Al<sub>2</sub>O<sub>3</sub>. Unit IV K-foidite (10AH041) forms a sub-parallel FeO(t)–CaO and Al<sub>2</sub>O<sub>3</sub>–CaO with respect to other samples of this group and shows the widest geochemical range (Fig. 6D and E).

The trace element contents obtained for the glasses from this group are up to 1000 times more enriched than primitive mantle (Fig. 7E). High ratios of LREE/HREE are expressed by La/Yb of between 90–114 for AH07A and 134–182 for 10AH062 (Table 3). The melt compositions also have high Ce contents (311–411 ppm; Table 3). There are also pronounced negative HFSE anomalies (Fig. 7E). There is also a range in

LREE/HFSE (Fig. 7A) and high Sr contents (AH07A = 1452–6527 ppm, Table 3; Fig. 7D).

#### 5.1.2. Leucite-rich K-foidite

This group consists of samples AH05 (Unit V) and 10AH07Sc1 (Unit VII). The glasses are classed as foiditic (48–53 wt.% SiO<sub>2</sub>, 13–16 wt.% Total alkalis; Fig. 5). The matrix glass of these samples has a large range in Na<sub>2</sub>O (7.2–10.5 wt.%) against a minimal range in MgO (0.2–0.5 wt.%; Fig. 6A). They also have lower K<sub>2</sub>O contents (6.5–8.3 wt.%; Fig. 6B). The glass also has the lowest CaO (2.6 wt.%) and FeO<sub>(t)</sub> (3.6 wt.%) contents of analysed Albano Maar samples (Fig. 6C). Relative to clinopyroxene- and leucite-rich samples, the glass compositions reflect a negligible variation in MgO and FeO<sub>(t)</sub> contents (Figs. 5D and 6C).

All of the glasses analysed are up to 1000 times more enriched than primitive mantle (Fig. 7E) and have high ratios of LREE/HREE (i.e. 10AH07Sc1, La/Yb = 109–570; Table 3). These glasses are also characterised by high incompatible element contents (i.e. La = 230 ± 26 ppm and Th = 110 ± 15 ppm, Table 3; Fig. 7A and C). The glasses also have larger negative HFSE anomalies (Fig. 7E).

#### 5.1.3. Transitional samples

Pumice clasts from Unit VI (10AH062) have matrix glass which has geochemical characteristics that are transitional between clinopyroxene- and leucite-rich, and leucite-rich K-foidites (Figs. 5 and 6). Unit VI matrix glass has higher Zr and Ti contents consistent with leucite-rich K-foidites (Table 2). The ratios La/Yb and Sr/Nd (75–420 and 43–98, respectively) are intermediate between the clinopyroxene- and leucite-rich K-foidites (La/Yb = 70–370; Sr/Nd = 22–126) and leucite-rich K-foidites (La/Yb = 109–570; Sr/Nd = 61 ± 12) (Table 3).

#### 5.1.4. Sanidine-rich phonolite

In contrast to the Albano Maar magmas described above, sample 10AH042 (Unit IV, Tables 3 and 4) is phonolitic (Na<sub>2</sub>O = 5.2–5.9 wt.%, SiO<sub>2</sub> = 57–58 wt.%; Fig. 6B) with low and uniform MgO contents (0.2–0.3 wt.%) and low CaO contents (2.7–3.3 wt.%; Table 2). The glass composition also has low Sr (1800 ± 109 ppm) and Ba (170 ± 7.4 ppm) contents, consistent with the presence of feldspar (Fig. 7E).

## 5.2. Phenocrysts

Representative phenocryst compositions are given in Table 4. The clinopyroxene found in these volcanic deposits is CaO-rich diopside-hedenbergite (Wo<sub>51</sub>En<sub>27</sub>Fe<sub>22</sub>–Wo<sub>42</sub>En<sub>39</sub>Fe<sub>13</sub>). The composition of the leucite does not depart from the ideal formula (KAlSi<sub>3</sub>O<sub>6</sub>) with a ratio of Si to Al close to 2:1; however in contrast, Unit IV (sample 10AH042) contains pseudoleucite and sanidine (An<sub>3</sub>Or<sub>42</sub>Ab<sub>55</sub>).

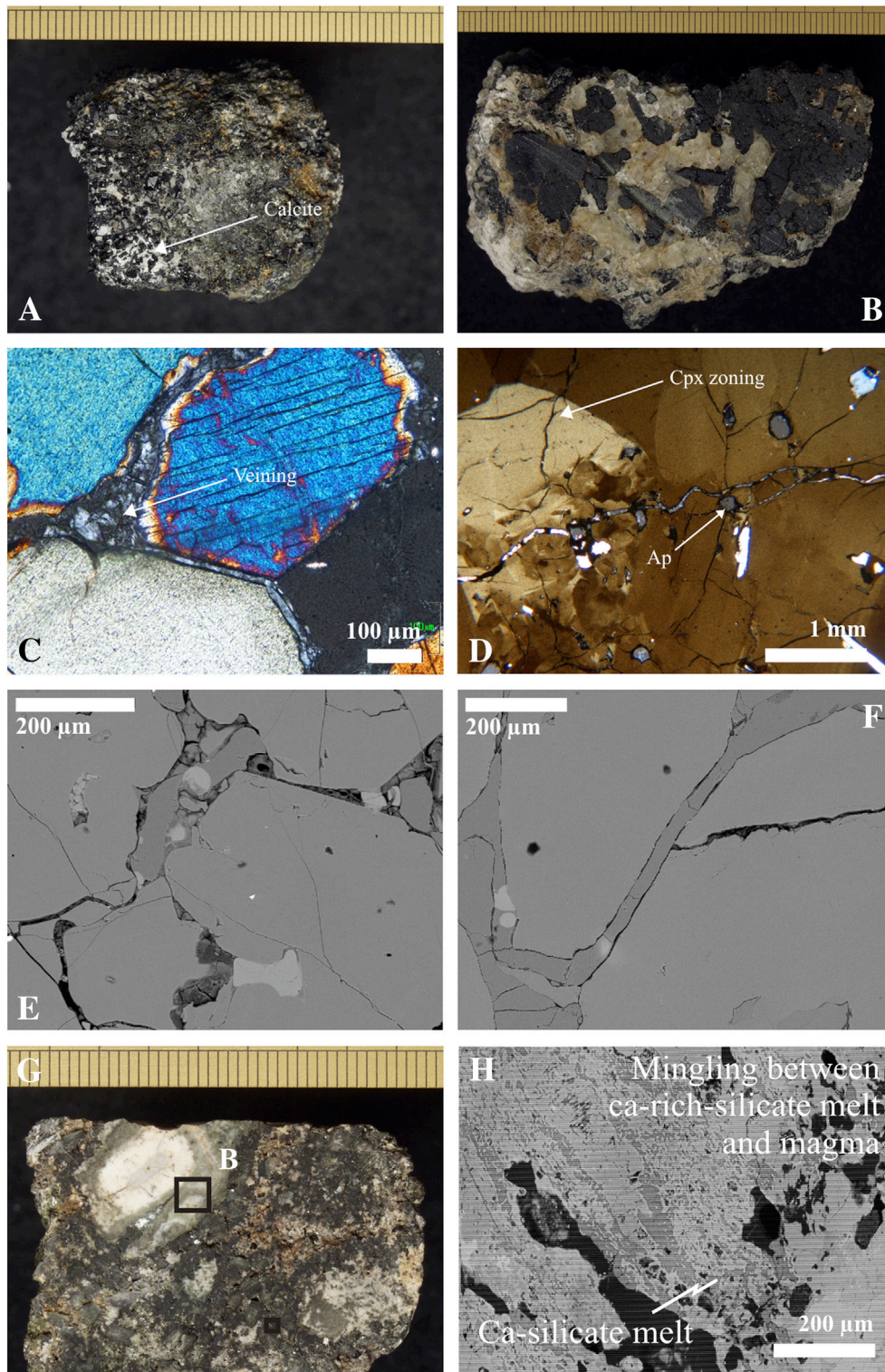


**Fig. 4.** Images of magmatic intrusive 10AH05cum (A) hand sample image; and (C) optical micrographs of veins and breakdown of clinopyroxene; and images of magmatic intrusive TG0mis (B) hand sample image; and (D) optical micrographs of zoned clinopyroxene and calcite. SEM (BSE) images of veins in 10AH05cum (E) and (F). (G) Photographed image of magmatic intrusive showing evidence for breakdown of skarn within the magmatic material (10AH05bc6), (F) BSE image of the same clast as (E) showing the mingling between a Ca-silicate melt emanating from the skarn and the magma. It is inferred that this Ca-rich melt is derived from upper crustal carbonate.

### 5.3. Magmatic intrusives

The intrusive clasts show evidence of interaction between magma and shallow carbonate. The clinopyroxenes are heavily zoned with a large number of apatite and calcite inclusions (Fig. 4C and D). Intrusive clasts are also affected by grain boundary breakdown and alteration by a

pervasive interstitial, Ca-rich glass (Fig. 4C and D), resulting in changes in birefringence at the crystal rims reflecting compositional variation. This melt has also taken advantage of cracks in crystals (Fig. 4C and D). In places, these cracks are filled with calcite.  $\text{CaCO}_3$  forms immiscible 'ovoid' shapes within the melt or has separated within the vein (Fig. 4E and F). There are no bubbles within the veins, indicating that the melt

**Table 3**  
Trace element analyses of proximal matrix glass (ppm). Data displayed are examples of single spot analyses that reflect the geochemical variation witnessed within glass of a single clast type. Full dataset provided in supplementary data.

Sample	10AH042			AH05	10AH062		AH07A		10AH07Sc1			10AH05cum	
Unit	IV			V	VI		VII		VII			VII	
No. of analyses	8 (34 μm)			6 (25 μm)	17 (34 μm)		4 (25 μm)		27 (34 μm)			5 (34 μm)	
SiO <sub>2</sub> <sup>a</sup>	59	58	58	51	51	50.3	50.8	52	52	51	52	0.02	1.07
MgO <sup>a</sup>	0.27	0.27	0.26	0.3	0.54	0.69	0.4	0.66	0.2	0.36	0.25	0.03	0.14
Na <sub>2</sub> O <sup>a</sup>	5.3	5.3	5.3	9.01	6.8	7.3	4.9	1.9	8.2	8.5	8.5	0	0
V	130	140	140	76	150	180	88	130	140	85	82	909	780
Rb	270	260	260	38	180	160	240	370	120	150	140	9	4.9
Sr	1700	1700	1800	7600	4020	4900	5300	4500	5400	5800	4900	2900	1300
Y	22	26	26	5.2	20.03	24	4.6	8.3	14	6	5.3	78	90
Zr	180	210	220	270	403	480	270	280	390	380	340	810	760
Nb	106	120	120	120	80.4	93	120	103	90	105	97	3.9	2.1
Ba	170	170	170	2400	1900	1600	2100	2800	2400	2600	2300	3.2	2.2
La	130	140	150	308	170	220	210	180	220	250	220	69	61
Ce	240	270	270	370	310	400	220	240	390	420	370	210	230
Pr	22	25	25	30	29	35	20	21	34	35	31	36	39
Nd	69	80	79	60.3	88	106	42	44	97	88	77	190	208
Sm	10.8	12	12	4.9	9.5	16	5.2	4.09	8.6	7.3	6.1	49	53
Eu	1.9	2.05	2.1	0.68	2.1	2.4	0.57	0.96	1.8	1.2	1	10.09	11
Gd	6.2	8	7.8	3.8	6.7	9.04	3.1	3.3	5.3	2.9	2.9	33	44
Dy	4.5	5.5	5.5	1.4	4.08	4.6	1.06	1.5	2.7	1.1	1.2	22	23
Er	2	2.4	2.3	0.77	2	2.3	0.7	0.71	1.2	0.47	0.47	7.3	8.8
Yb	1.7	2	2	0.73	1.7	1.9	0.57	0.92	0.97	0.45	0.601	5.4	6.6
Lu	0.24	0.29	0.29	0.23	0.28	0.27	0.18	0.16	0.17	0.1	0.12	0.84	0.89
Ta	5.03	6	6.1	3.6	2.9	3.3	3.2	3.2	3.3	3.8	3.3	0.95	0.66
Th	45	52	53	140	90.8	110	120	101	103	120	103	2.2	4.3
U	18	21	22	39	30.1	39	<LOD	31	39	46	42	0.91	1.2

<sup>a</sup> Major element data (wt.%) relative to the specific areas analysed for trace elements.

has completely degassed or volatiles were still dissolved in the melt when it was quenched, without ability for exsolution. Breakdown and mingling of skarn material (Ca-silicate-melt) are also observed within a few of the samples (Fig. 4G and H).

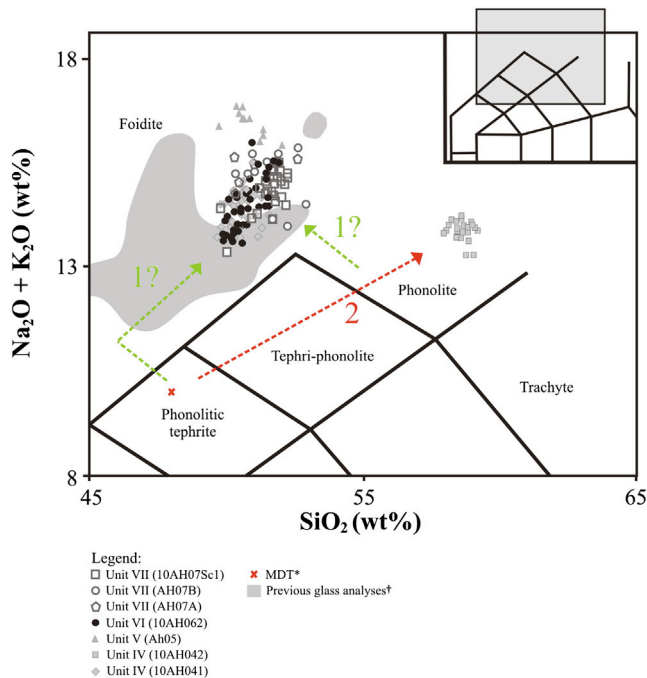


**Fig. 5.** Total alkalis vs silica (TAS) diagram of all matrix glass data. Lava analysis from the Monte Due Torri scoria cone (MDT; Whole rock (WR); Gaeta et al., 2011) defines the most primitive melt composition in this study. The arrows reflect experimentally determined evolutionary paths (1) 1–2 wt.% H<sub>2</sub>O and CaCO<sub>3</sub> at 0.5 GPa; and (2) up to 2 wt.% H<sub>2</sub>O only, at 0.5 GPa from Freda et al. (2008). † Matrix glass data of De Benedetti et al. (2008), Freda et al. (2006), and Giacco et al. (2007, 2008).

### 5.3.1. Ca-rich glass

The Ca-rich glass has low WDS-EPMA totals (55–70 wt.%; Table 2). The glass contains 55–70 wt.% CaO, with 1 wt.% of SiO<sub>2</sub>, Al<sub>2</sub>O<sub>3</sub>, FeO<sub>t</sub>, MgO and alkalis (Table 2). The deficit is between 30 and 45%. This deficit is the equivalent of the stoichiometric CO<sub>2</sub> content of CaCO<sub>3</sub> and similar to that in analysed carbonatitic compositions (Brooker and Hamilton, 1990). All of the glasses analysed are compositionally homogeneous across the veins and between the magmatic intrusives within which they were analysed.

### 5.4. Summary

Albano Maar glasses, representative of the erupted melts (Units IV–VII; 41 to 33 ka) are characterised by:

- > Foiditic compositions, with the clinopyroxene and leucite-rich and leucite-rich magmas forming separate populations, with a transitional sample and the occasional occurrence of phonolitic composition
- > Positive correlations between CaO, FeO<sub>t</sub> and MgO, at high K<sub>2</sub>O contents (6–14 wt.%)
- > High LREE/HREE ratios, which allow the ability to distinguish between glasses of different samples
- > Large negative HFSE depletions (Nb, Ta and Ti) and large enrichments in Pb and Sr
- > Glass compositions differ between different pumice clasts within different stratigraphic levels of the same erupted unit, thus proving the importance of studying each individual pumice clast found, rather than focussing upon the initial erupted phase.

Magmatic intrusive clasts show evidence for interaction with carbonate and contain pervasive interstitial, Ca-rich glass.

## 6. Discussion

The discussion will cover various aspects of the Albano Maar deposits to investigate crustal and eruptive processes and dispersal of volcanic ash.

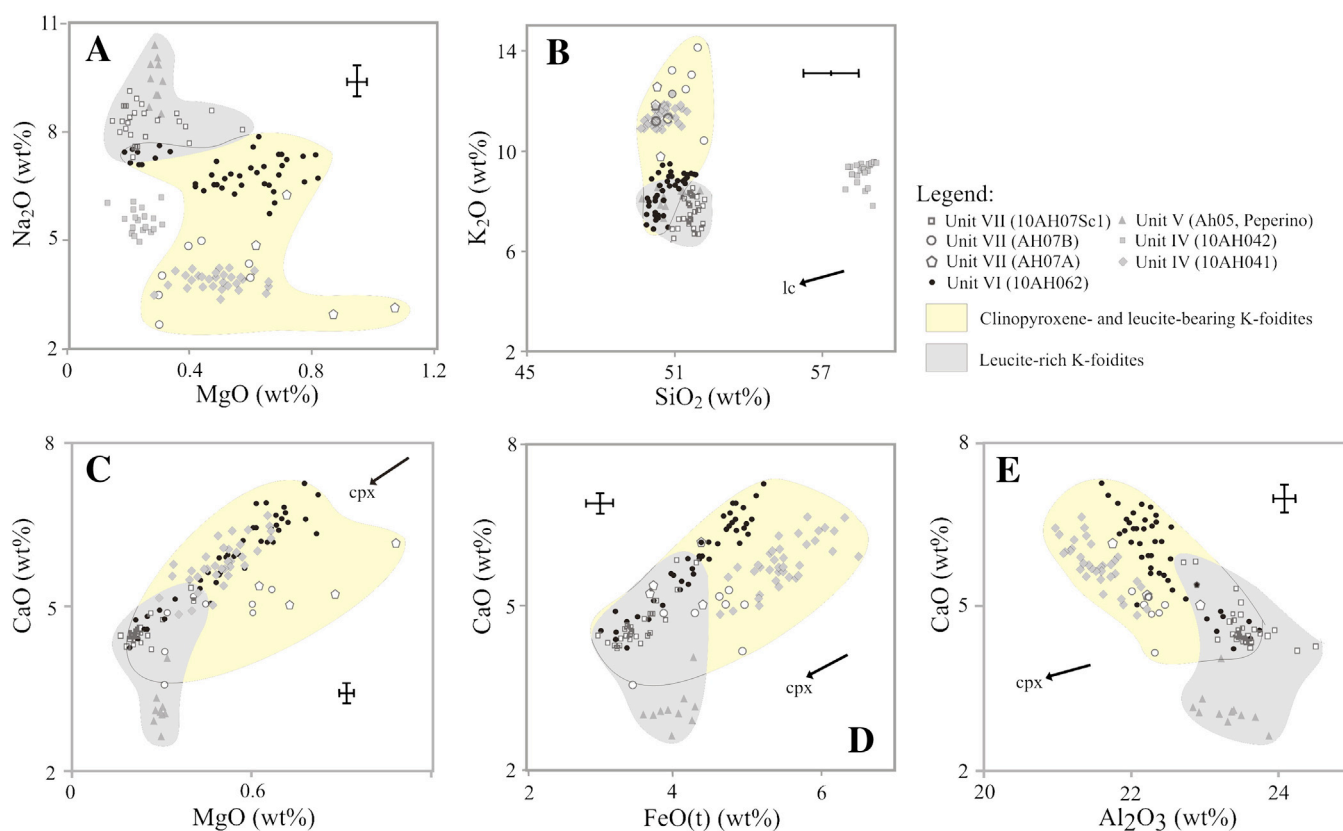


**Fig. 6.** Major element composition of matrix glass. Mineral phase vectors are shown, calculated from in situ analyses of mineral phases from the same juvenile clasts. All error bars are  $\sim 2\sigma$ , representing the precision on MPI-DING standard StHs6/80-G glasses.

### 6.1. Geochemical variation in juvenile pumice matrix glass chemistry

Matrix glass of the Albano Maar juvenile clasts has high LREE/HREE ratios, and is depleted in HFSE (Nb, Ta and Ti; Fig. 7E), which is typical of convergent settings (e.g. Avanzinelli et al., 2008, 2009; Boari et al., 2009; Conticelli et al., 2010 and the references therein). Deep mantle geochemical signatures however may be overprinted during subsequent storage and differentiation. Here we assess the relative importance of crustal contamination and fractional crystallisation on the composition of Albano Maar magmas.

The basement beneath Albano Maar provides a large range of conditions through which the conduit system has plumbed and excavated. A series of experimental studies provide a better understanding of the magmatic history of the unusual foiditic magma compositions erupted at Albano Maar. These experiments were performed on both plagioclase-free phono-tephrite (Marra et al., 2003) and the most primitive K-basalt outcropping in the RMP (Peccerillo, 2005). Experimental conditions varied from anhydrous, hydrous to hydrous-carbonated at 1 atm, 500 MPa and 1000 MPa (Freda et al., 2008; Iacono-Marziano et al., 2007, 2008; Mollo et al., 2010). Experiments conducted at 500 MPa produce melt compositions with textures and phase relations that closely resemble those of the Albano Maar magmas (Freda et al., 2008). All of these experiments furthermore indicate that adding  $\text{CaCO}_3$  to the starting material drastically changes phase relations (Freda et al., 2008; Iacono-Marziano et al., 2007, 2008; Mollo et al., 2010).

With  $\text{CaCO}_3$  as a crustal contaminant, the crystallisation of Ca-rich clinopyroxene is favoured and magnetite and phlogopite stability fields are strongly reduced due to the decrease in  $\text{H}_2\text{O}$  solubility, caused by the large input of  $\text{CO}_2$  from decarbonation reactions. As a result, the residual melt is strongly silica-depleted, favouring the formation of foiditic melts as shown by our dataset (Fig. 5) (Freda et al., 2008; Gaeta et al., 2009; Iacono Marziano et al., 2007, 2008, 2010; Martelli et al., 2004; Mollo

et al., 2010). Carbonate assimilation is recorded as a decrease in  $^{87}\text{Sr}/^{86}\text{Sr}$  isotope ratio of the magmas because of the low  $^{87}\text{Sr}/^{86}\text{Sr}$  isotope ratio of the Mesozoic carbonates (Boari et al., 2009). It must be noted that such a process of dilution involves a significant drop in temperature and hence significant pre-eruptive crystallisation at depth, this may help to explain why such highly crystallised clasts have erupted at Albano Maar (Fig. 3). Without the input of  $\text{CaCO}_3$  and in the presence of  $\text{H}_2\text{O}$ , olivine and plagioclase feldspar would crystallise. The melt therefore follows a more traditional magmatic evolution towards a phonolitic composition (Gaeta et al., 2006; Iacono Marziano et al., 2007, 2008; Melzer and Foley, 2000).

Albano Maar glass compositions can be compared with the experimental trends of Freda et al. (2008) in Fig. 5. If we assume a starting composition represented by the least evolved MDT lava erupted in the Colli Albani Volcanic District (erupted from the Monte Due Torri scoria cone; Gaeta et al., 2011), the dominant evolutionary Path 1 of Albano Maar magmas is within the foiditic field, which suggests a high partial pressure of  $\text{CO}_2$  (1–2 wt.%  $\text{H}_2\text{O}$  + 1–5 wt.%  $\text{CaCO}_3$ ; Fig. 5). In contrast, Path 2 towards phonolite (Fig. 5) reflects a low partial pressure of  $\text{CO}_2$ . However, there is only one clast type in Unit IV containing melt (glass) consistent with evolution along Path 2 towards phonolite (1–2 wt.%  $\text{H}_2\text{O}$ ; sample 10AH042; Fig. 5). Two options for evolutionary Path 1 are shown in Fig. 5 based upon the timing of contamination relative to crystallisation. Examples shown include (a) contamination of a relatively unfractionated phonolitic tephrite, and (b) contamination of a highly fractionated phonolite. In both instances, foiditic compositions are the end result.

#### 6.1.1. Evolutionary Path 1 (K-foidite)

**6.1.1.1. Crustal contamination.** The abundance and relative proportions of different lithic components within the erupted deposits provide evidence for shallow carbonate interaction with the Albano Maar magmas

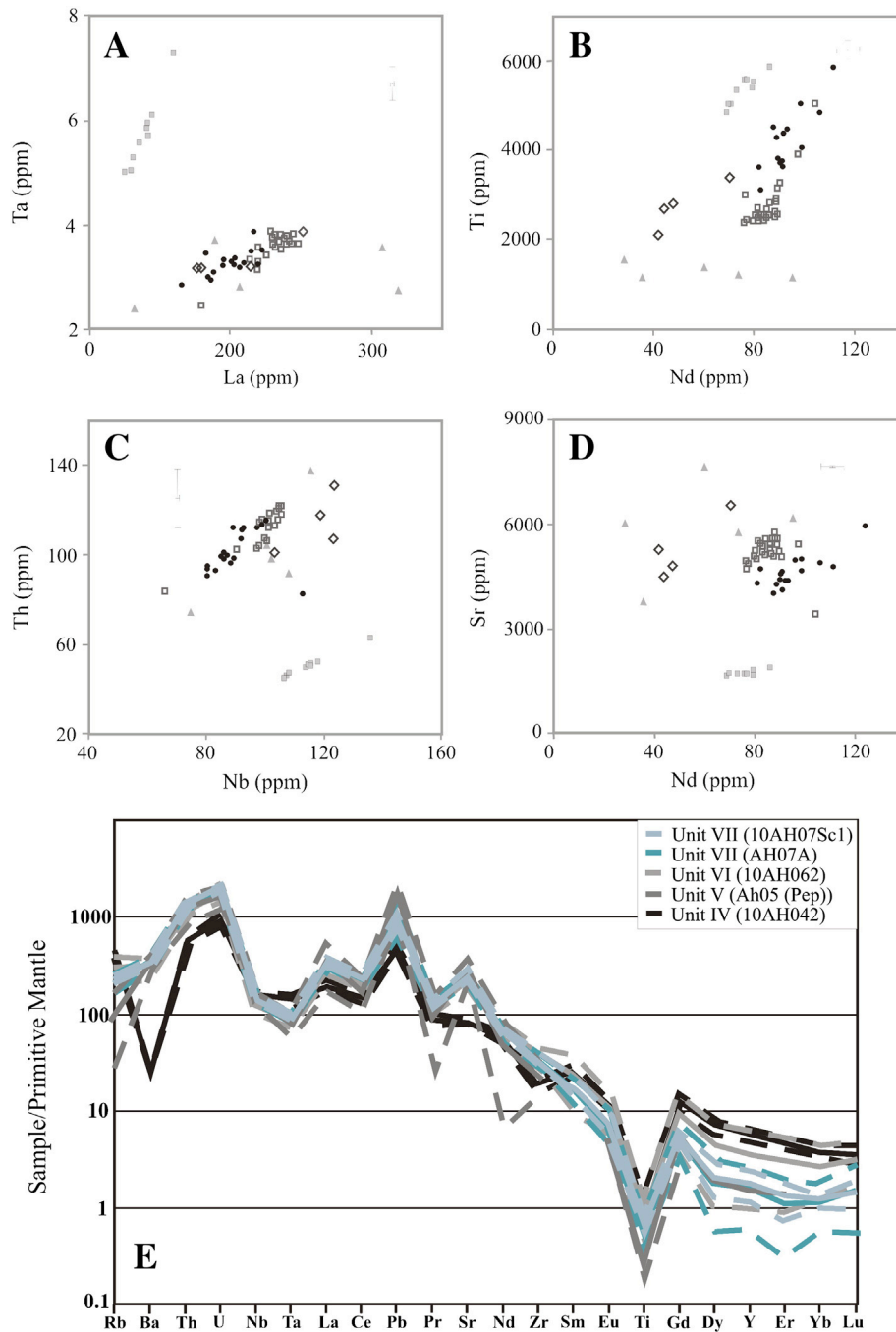


**Fig. 7.** (A) Multi-element diagram of proximal glass analyses normalised to Primitive Mantle (Sun et al., 1989). Trace element compositions of matrix glasses. All error bars represent  $\pm 2\sigma$ , which reflects uncertainty of determination of the MPI-DING standard StHs6/80-G.

(Fig. 8A). Carbonate is witnessed having interacted with magmatic material in the Albano Maar deposits (Fig. 4; De Benedetti et al., 2008, 2010; Di Rocco et al., 2012; Sotilli et al., 2008).

To test the effect that late-stage contamination has on the composition of the residual melts, we have modelled simple mixing between the Ca-rich melt (55–70 wt.% CaO, from magmatic intrusive 10AH05cum) and the least contaminated glass composition (from pumice sample 10AH07Sc1, Unit VII; Fig. 8B–G). Mixing is supported by compatible-compatible element and compatible-incompatible ratio plots. In a two component system, mixing is linear if the denominators of the ratios are the same. Intermediate points along the hyperbola indicate the relative proportions of each end-member and therefore should lie on a straight line on a companion plot of one of the original ratios vs the ratio of the denominators of the two original ratios (Langmuir et al.,

1978, the equation derived from the form  $Ax + Bxy + Cy + D = 0$ ). As we do not know the geochemical data for the end members (more primitive magma and carbonate) instead we investigated the impact that mixing between the juvenile pumice glass and Ca-rich melt has upon the variation in pumice glass composition. Matrix glass compositions from Albano Maar pumice clasts plot on or close to the calculated mixing lines (i.e.  $Al_2O_3$ –CaO,  $SiO_2$ –CaO and Sr–Nd), suggesting mixing of ca. 50% of Ca-rich melt with the magma (Fig. 8B–E). There is clear variation in the amount of mixing/contamination experienced by melt erupted within a single eruption (e.g. 10AH062, Unit VI 0–50% mixing).

The formation of a Ca-rich-silicate melt has been suggested as a product of the ultra-potassic magma–carbonate interaction (Gaeta et al., 2006, 2009), and that it is this melt that then contaminates the rest of the magma body via an endoskarn at the contact between

**Table 4**

Representative phenocryst compositions (wt.%).

	Unit IV			Unit V	Unit VI	Unit VII		
	<u>10AH041</u>	<u>10AH042</u>		<u>AH05</u>	<u>10AH062</u>	<u>AH07A</u>	<u>AH07B</u>	<u>10AH07Sc1</u>
	Clinopyroxene	Sanidine	Leucite	Leucite	Leucite	Leucite	Clinopyroxene	Leucite
SiO <sub>2</sub>	44.32	63.77	55.76	53.21	53.69	54.35	40.2	53.58
TiO <sub>2</sub>	1.66	0.06	<LOD	0.05	0.12	0.05	2.16	0.08
Al <sub>2</sub> O <sub>3</sub>	9.1	19.93	22.81	23.98	24.15	24.86	12.3	23.21
FeO <sub>(t)</sub>	10.06	0.5	0.57	0.34	0.77	0.44	13.56	0.65
MnO	0.16	<LOD	<LOD	0.02	0.02	<LOD	0.27	0.01
MgO	10.15	0.01	<LOD	<LOD	<LOD	<LOD	7.45	<LOD
CaO	24.04	0.48	<LOD	0.14	0.12	0.06	23.59	0.13
Na <sub>2</sub> O	0.29	2.77	0.5	0.72	0.88	0.76	0.23	0.28
K <sub>2</sub> O	0.02	11.86	20.01	20.14	19.86	20.38	<LOD	21.01
Total	99.79	99.37	99.64	98.74	99.59	101.08	99.77	98.96
Si	2	2.3					1.9	
Ti	0.04	<LOD					0.06	
Al	0.43	1.07					0.59	
Cr	<LOD	<LOD					<LOD	
Fe <sub>2</sub>	0.25	0.01					0.34	
Mn	<LOD	<LOD					<LOD	
Mg	0.52	<LOD					0.4	
Ca	0.76	0.02					0.76	
Na	0.02	0.17					0.01	
K	<LOD	0.44					<LOD	
W <sub>o</sub>	42	–					51	
En	39	–					27	
Fs	13	–					22	
An	–	3					–	
Or	–	42					–	
Ab	–	55					–	

Cations calculated O for clinopyroxene and sanidine.

magma and carbonate (Di Rocco et al., 2012; Gaeta et al., 2006, 2009). Recent experimental work on products of Merapi volcano, has also inferred the formation of a Ca-silicate melt during carbonate breakdown (Deegan et al., 2010). However, actual evidence of the existence of Ca-rich melts formed at shallow depths has not been reported until now. Evidence for a Ca-silicate melt has been found mixing/mingling with partially crystallised silicate magma in Albano Maar samples (Fig. 4G and H).

**6.1.1.2. Crystal fractionation.** The juvenile pumice clasts (Fig. 3) from the Albano Maar units have high crystallinity (60–80%; Table 1). The clasts range from clinopyroxene and leucite-rich to leucite-rich and follow different liquid lines of descent (Fig. 5). It would therefore be expected that the residual matrix glass chemistry would follow crystal vectors calculated based on the chemistry of the crystal phases from the same juvenile clasts (Fig. 6B–E). Instead the data follows straight lines and does not agree with all of the clinopyroxene or leucite vectors (Fig. 6). The matrix glass from clasts of Unit V however, follows the leucite vector.

Compositional variation within a single clast type is seen for several of the contaminated units (CaO, FeO<sub>t</sub> and MgO; Fig. 4A, C, D and E). These clasts show little variation in SiO<sub>2</sub> and K<sub>2</sub>O, indicating that small scale differences in composition are not caused by crystallisation (in this case leucite). Instead the majority of variation appears to be associated with late stage mixing/contamination prior to eruption. This is based upon the understanding that in a silicate melt  $D_{Na} > D_K > D_{Ca} > D_{Al} > D_{Si}$  (Jambon, 1983), therefore the variations in composition do not reflect different diffusivity. For example, glass analyses from Unit VI have the highest CaO and MgO contents and the largest range in these contents, in agreement with the largest and most varied interaction with the Ca-rich melt (Figs. 5 and 8). Recent work has shown that late-stage contamination is relevant only for small volume magma chambers at the Colli Albani Volcanic District, i.e. post-caldera activity (Boari et al., 2009; Conticelli et al., 2010; Giordano et al., 2006). It is possible to infer that magmas at Albano Maar are contaminated multiple times during magma evolution: Early contamination is indicated by

experimental evidence for CaCO<sub>3</sub> input forcing the crystallising phases and hence evolution towards foiditic compositions (Freda et al., 2008), while this study provides evidence for late-stage contamination, in the form of physical mixing in hand-specimens and chemical mixing with Ca-rich melt, which masks prior evidence for fractionation and complicates equilibrium between crystals and melt. The only samples that do show variation consistent with fractionation are AH07A and AH07B (belonging to Unit VII, the last known erupted unit). It is important to also note, that due to the crystal-rich nature of these samples, crystal re-equilibration and contamination could have occurred in the magma, however late stage mixing will have also masked any potential geochemical signature.

**6.1.1.3. Volatile input and degassing.** The Ca-rich melt veining analysed in the magmatic intrusives has a 60:40 ratio of melt to volatile contents consistent with a carbonatitic material (Brooker and Hamilton, 1990; Brooker and Kjaarsgaard, 2011 and the references therein). It has also been suggested that an increase in Ca<sup>2+</sup>, Na<sup>+</sup> and K<sup>+</sup> in the melt increases the dissolution of CaCO<sub>3</sub> and storage of CO<sub>2</sub> in shallower regions, which is not affected by temperature (Lowenstern, 2001 and the references therein). The generation of shallow derived carbonatitic melts allows for a significant increase in CO<sub>2</sub> storage in the silicate system.

A crucial question relating volatile input from Ca-rich melt with magma evolution and explosivity, is how much of the released CO<sub>2</sub> could be stored under magma chamber conditions? CO<sub>2</sub> solubility is very low at shallow crustal levels (<100 ppm solubility of total CO<sub>2</sub> in alkali-rich magmas at 300–500 MPa; Lowenstern, 2001). However, recent experimental work on Colli Albani Volcanic District magmas, has shown that CO<sub>2</sub> solubility is much greater than previously perceived (~0.1–0.3 wt.%; Behrens et al., 2009) under the conditions suggested for magma storage (200–300 MPa). Although CO<sub>2</sub> solubility is significantly higher in phono-tephritic melts than in silicic to mafic melts, the capacity for dissolving carbonate is nevertheless low at shallow *P–T* conditions. The same study showed that an increase in CO<sub>2</sub> solubility is consistent with H<sub>2</sub>O solubility meaning that an input of CO<sub>2</sub> does not necessarily decrease H<sub>2</sub>O solubility. This observation is thought to be

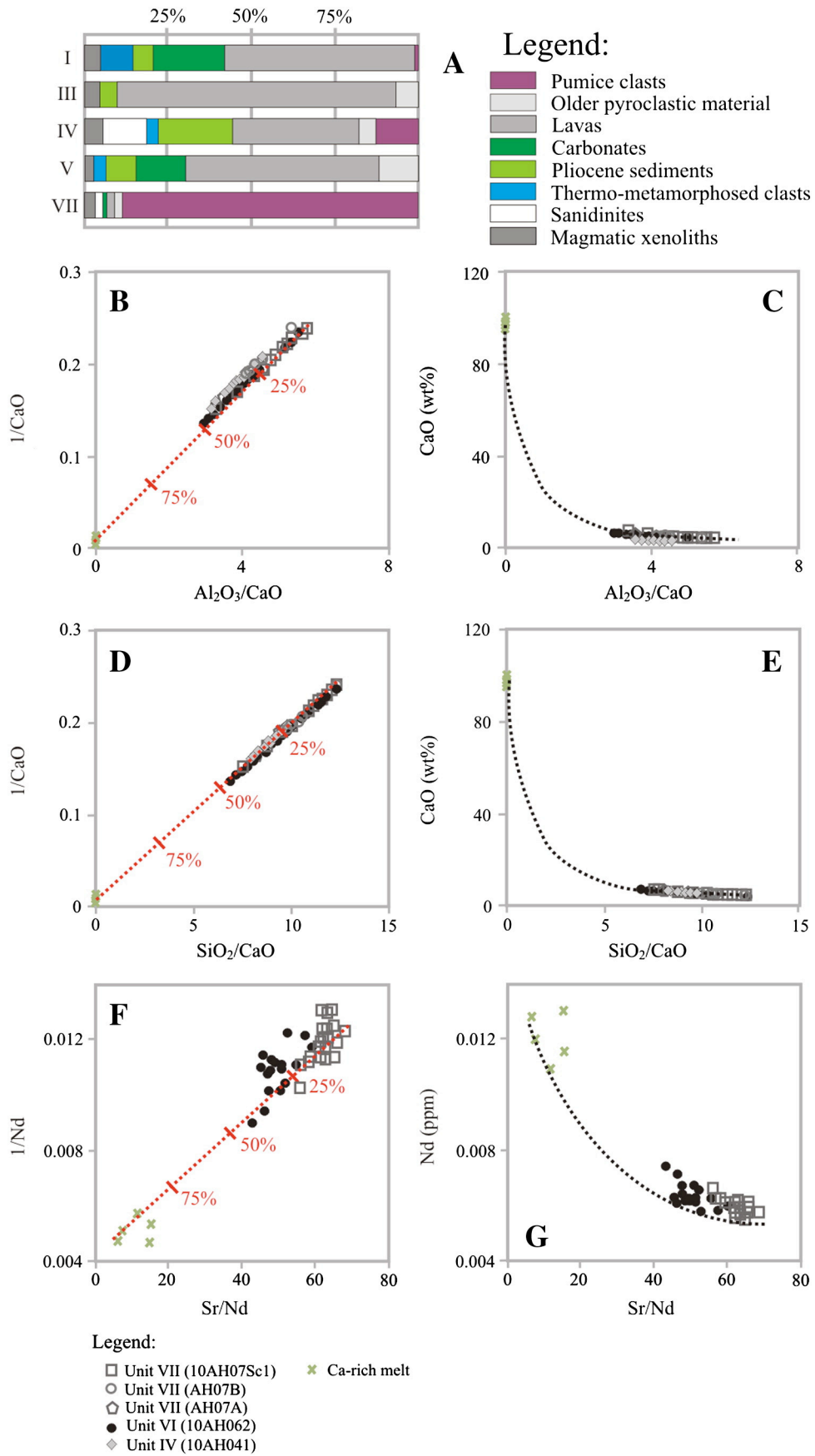


**Fig. 8.** (A) Histogram of the types of clasts found in the eruptive units of Albano Maar. Ratio vs ratio plot, inferring straight line mixing between Ca-rich melt and juvenile glass for (B)  $Al_2O_3/CaO$  vs  $1/CaO$ , (D)  $SiO_2/CaO$  vs  $1/CaO$  and (F)  $Sr/Nd$  vs  $1/Nd$ . Alongside these plots are their companion plots that define data falling along a mixing line (C, E and G).

due to the resultant modification of the melt structure created by H<sub>2</sub>O, increasing the capacity for the incorporation of CO<sub>2</sub> (Behrens et al., 2009; Botcharnikov et al., 2006). The different experimental runs in the study by Behrens et al. (2009) show that for a melt containing 2.3 wt.% H<sub>2</sub>O and 0.21 wt.% CO<sub>2</sub>, it will start to degas at 1250 °C when the pressure drops below 200 MPa, producing a separate CO<sub>2</sub>–H<sub>2</sub>O fluid. The composition of this fluid is not well constrained, however it provides support for the further mobility of volatiles in the system.

The impact and timing of this contamination between eruptions at Albano Maar can also be inferred from the timing of degassing relative to crystallisation. Clasts from Unit V (Fig. 3C) differ texturally to the rest of the pumice clasts erupted from Albano Maar (Fig. 3A, B, D, E and F). They are the only clasts to have undergone pre-degassing crystallisation of leucite (Fig. 3C) and they do not have glass compositions that follow the same mixing line between silicate magma and Ca-rich melt (Fig. 8). The rest of the clasts analysed instead have undergone syn-degassing ascent driven crystallisation of leucite. There is contention as to whether or not syn-microcrystallisation impacts upon the residual melt chemistry (Shane et al., 2008) and the evidence from these samples suggests little geochemical impact via a leucite influenced geochemical trend (Fig. 6).

A good example of the variation in the timing of crystallisation and degassing is provided by the different juvenile components of Unit VII. The first erupted sample (AH07A; Unit VII; Fig. 9A and B) reflects both pre-degassing (eruptive) crystallisation with a small number of equant leucite microcrysts. However, the clasts are also predominantly impacted by syn-degassing (eruptive) crystallisation of leucite that has affected the shape of the vesicles (equant shape, aspect ratio 1:1.25:1.6; 60% vesiculation). The second erupted sample AH07B (Unit VII; Fig. 9C and

D), however, has undergone only syn-degassing crystallisation. The black and white image shows the lower vesicularity and also alteration of the vesicle shape during growth, although the vesicle size distribution is the same as AH07A (Fig. 9G and H). Furthermore, the final erupted sample 10AH07Sc1 also shows syn-degassing crystallisation (Unit VII; Fig. 9E and F) but with no evidence for vesicle deformation caused by crystallisation (equant shape, with aspect ratio 1:1.25:1.25). What is also evident from the VSD of sample 10AH07Sc1 is a change from steady state degassing of a single vesicle population (samples AH07A and AH07B) to interconnection becoming more dominant, this could be due to a decrease in ascent rate, indicative of degassing commencing from a shallower level of the crust (Cross et al., 2012).

These differences in the texture of erupted juvenile clasts have also been witnessed in products from Vesuvius. Recent experimental work by Shea et al. (2009) has demonstrated that differences in crystal habit with relation to vesiculation are caused by changes in storage time and volatile ratios of melt of differing viscosities in the shallow crust (Shea et al., 2009; Vinkler et al., 2012). The increase in syn-eruptive crystallisation is caused by an increase in XH<sub>2</sub>O within the magma. This evidence indicates that these different clast groups must have been stored under varied conditions in terms of pressure, temperature and volatile variations. These different paths of ascent have impacted on the late stage microcrystallisation, however studies also suggest that there is initial compositional control on the extent of this crystallisation (Blundy and Cashman, 2001). The less evolved the magma before the onset of degassing and syn-eruptive crystallisation, the larger the percentage of crystallisation. This agrees with the decrease in syn-eruptive crystallisation of the erupted clasts of Unit VII, up through the eruptive stratigraphy.

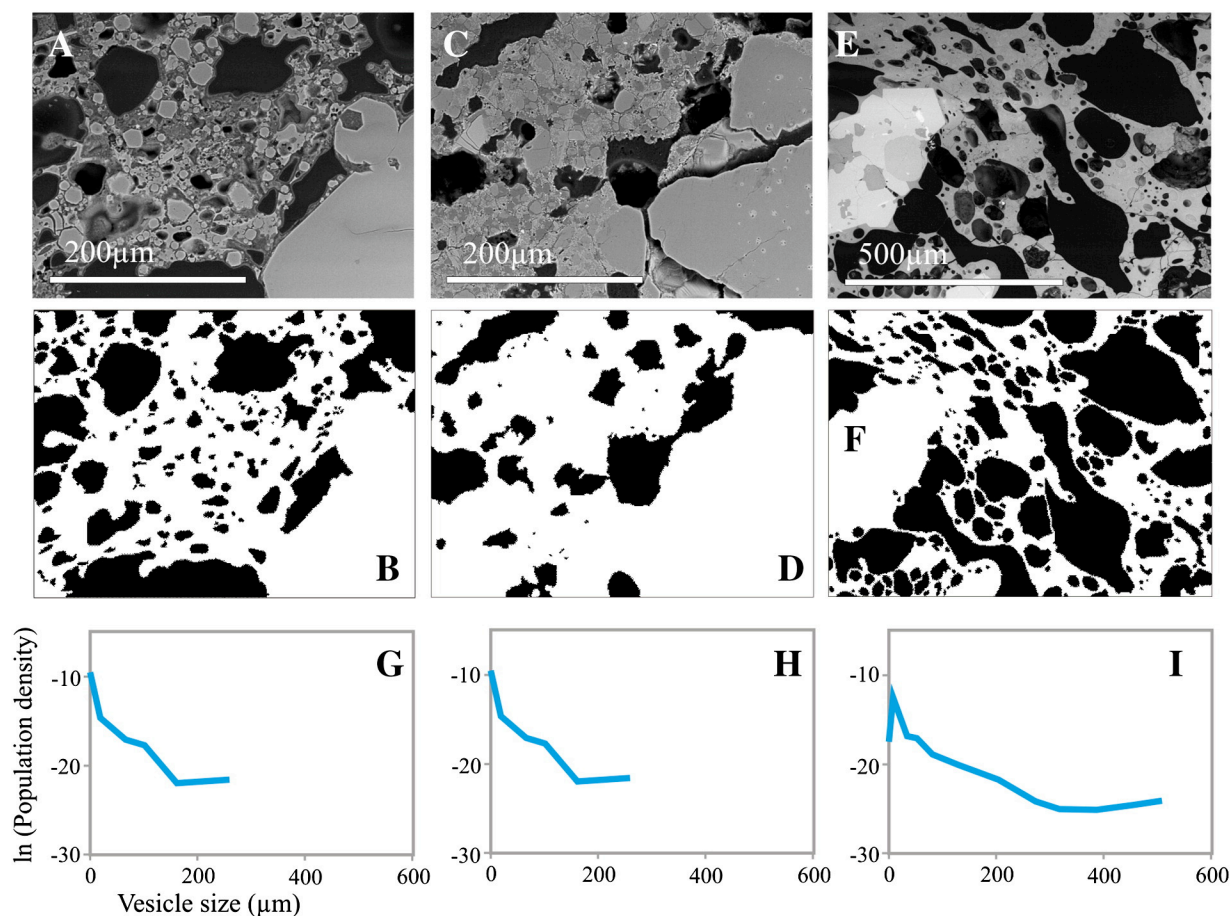


**Fig. 9.** BSE (SEM) images and black and white versions of the original of samples to calculate vesicle size and distribution (F, G, H; see Cross et al., 2012 for method). (A), (B) & (F) Unit VII (AH07A); (C), (D) & (G) Unit VII (AH07B); (E), (F) & (H) Unit VII (10AH07Sc1).

**6.1.1.4. Explosivity.** Experimental work on magma–carbonate interaction with magmas at Merapi (Deegan et al., 2010) has shown that sudden volatile exsolution can occur at the interface between Ca-rich melt and silicate magma. This highlights the potential importance of Ca-rich and silicate-melt interaction for variations in magma explosivity and eruptive style.

In this study evidence for ~50% mixing between juvenile silicate magma and a Ca-rich melt is recorded (Fig. 8). Based upon the assumed volatile content (CO<sub>2</sub>) of the Ca-rich melt from stoichiometric understanding and the established amount of CO<sub>2</sub> that can be dissolved in the magma in shallow magma chamber conditions (0.1–0.3 wt.%, Behrens et al., 2009), it can be inferred that this mixing event would create a fluid or free volatile phase of ~20 wt.% of the resulting total. Instantaneous release of this fluid/free volatile phase could co-exist with the magma and may provide enough of a pressure change within the magma chamber to trigger eruption.

The predominance of syn-degassing crystallisation in the juvenile clasts during ascent also suggests significant volatile exsolution on ascent. Furthermore, the volatile content was high enough that it was able to drive explosive eruption rather than viscous death following crystallisation. We therefore infer that the late-stage Ca-rich contamination event supplied a large enough volume of volatile to trigger and increase the explosivity of eruption.

#### 6.1.2. Evolutionary Path 2 (phonolite)

Unit IV (ca. 41 ka; Gaeta et al., 2011) contains a clast type with a matrix glass composition consistent with evolution along Path 2 (from phonolite–tephrite to phonolite, with up to 2 wt.% H<sub>2</sub>O and low CO<sub>2</sub>) (Fig. 5). Unit IV has a high proportion of Pliocene sediment lithics (18%), hornfelses (thermo-metamorphosed sediments; <2%) and sanidinities (10%) than is seen within any other Albano Maar units (Table 1). This supports greater interaction between Unit IV magmas and siliceous sediments, rather than with carbonate. Indeed, the Unit IV phonolite has elevated HFSE (Ta and Ti) and depleted LREEs, Sr and Ba, relative to the K-foiidite magmas. The experimental work of Freda et al. (2008) suggests that in the absence of carbonate, magnetite and phlogopite crystallise at relatively high temperatures and this drives the glass composition towards silica enrichment, resulting in a differentiation trend moving from phono-tephritic to phonolitic compositions. Additionally the decreased CO<sub>2</sub>/H<sub>2</sub>O ratio favours the crystallisation of feldspar. This Unit IV phonolite contains both sanidine (K-feldspar) and phlogopite mica alongside clinopyroxene (Table 1). This provides further evidence for changes in the contaminant impacting upon the crystal phases that can crystallise during magma evolution. The evolution towards phonolite is rare in this system because of the predominance of carbonate in the shallow crust (1–6 km), meaning magmas must have evolved deeper within the crust or in gaps within the carbonate crust.

#### 6.2. Constraints on eruption age

The main geochemical signature of Albano Maar magmas is predominantly foiditic, with rare phonolite (12–18 wt.% total alkalis and 48–52 wt.% SiO<sub>2</sub>), high enrichment in LREEs, with a large range in LREE/HREE contents (La/Yb = 75–480), and with HFSE depletions (narrow range in Nb/Ta = 19–38). To better understand the dispersal of volcanic ash from Albano Maar, we analysed the major and trace element glass composition of several distal tephra layers preserved in the Lago Grande di Monticchio (LGdM) core that were previously ascribed to Albano Maar. The TM-17 distal units (TM-17a, TM-17b, TM-17c, d and TM-17e) have juvenile glass clasts/shards that are basaltic-trachy-andesite to phonolitic tephrite in composition. TM-17bc is the only distal layer that geochemically correlates to an Albano Maar Unit VI (Fig. A, supplementary material) on both foiditic major and trace elements. TM-17bc is dated by the Monticchio chronology at 31,830 ± 1590 varve yrs BP (Wulf et al., 2012). This date, however, is

considered ca. 3000 yrs too young as estimated from the varve ages and ages of major tephra correlatives of underlying (Campanian Ignimbrite) and overlying (Y-3, Codola) distal tephra deposits (Wulf et al., 2012). Thus, we assume an age of ca. 35 ka BP by incremental dating for the Unit VI eruption, which is in agreement with the <sup>40</sup>Ar/<sup>39</sup>Ar ages of proximal Unit V obtained by Freda et al. (2006) and Giaccio et al. (2009).

#### 6.3. Magmatic implications

The Albano Maar glasses analysed in this study seem to belong to two experimentally determined separate evolutionary paths. In the presence of H<sub>2</sub>O and without CaCO<sub>3</sub> assimilation, magmas have evolved towards a phonolitic composition. However the majority of the Albano Maar magmas analysed are foiditic in composition, which evolved in the presence of CaCO<sub>3</sub>. The resulting CO<sub>2</sub> saturation influenced the fractionation path of the foiditic magmas, leading to silica-undersaturation and alkali enrichment. Geochemical analysis of these glasses however also reflects a late-stage contamination event with a Ca-rich melt inferred to have originated from the basement carbonate (i.e. CaCO<sub>3</sub>). It is therefore likely that CaCO<sub>3</sub> contamination of the foiditic magmas was occurring before, during and after the main phase of fractional crystallisation.

Differences in matrix glass chemistry between the studied post-caldera Albano Maar products can therefore be attributed to variations in liquid lines of descent, which are controlled by spatial and temporal differences in melt storage and hence conduit structure. Fig. 10 schematically illustrates the potential temporal changes in the architecture of the Albano Maar volcanic conduit. This is inferred from changes in the volume of different lithic components of each eruption (Fig. 8A; De Benedetti et al., 2010), pumice clast texture (Fig. 3) and melt chemistry (Figs. 5, 6 and 7). For the purpose of the following discussion, it is assumed that the extent of the carbonate contamination is negatively correlated with magma volume and positively correlated with residence time. In addition, we assume an ability for repeated contamination events through time that have not necessarily triggered eruption. This is supported by work completed by Boari et al. (2009) and Giordano and CARG Team (2010). The Albano Maar units are small volume, so we envisage that differentiation processes may be fast and ongoing during the rise at shallow depth of small batches of magmas, which fed each eruption.

##### 6.3.1. Unit IV (ca. 41 ka)

Unit IV contains two different types of pumice clast: K-foiidite, which evolved in the presence of CaCO<sub>3</sub> and phonolite, which instead evolved in H<sub>2</sub>O-rich, CO<sub>2</sub>-poor conditions (Fig. 5). This would suggest that there is magma storage in at least two regions, one below the stratigraphic level of crustal carbonate, and one within it (Fig. 10A). Unit IV is a small volume eruption, with a small percentage of juvenile pumice clasts (Fig. 8A). We therefore suggest that there were small volume magma batches with an increased surface area interacting with the wall rock, leading to increased contamination. Mixing calculations (using equations determined by Langmuir et al., 1978) have predicted efficient mixing and contamination with the foiditic melt (10AH041, ~25% mixing). However this contamination must have been late stage as (a) it postdates fractional crystallisation, overprinting any geochemical signature that would have been shown by this process, and (b) un-hybridised, mingled clasts are found in the deposits. The eruptive style was base surge followed by ballistic fallout suggesting a volatile-driven eruption.

##### 6.3.2. Unit V (ca. 36 ka)

The erupted deposit Unit V (Peperino ignimbrite) is extremely fragmented, and unaltered pumice clasts are rare. This unit has the largest volume of all of the Albano Maar units and has an associated pyroclastic density current deposit, indicative of a large volume magma

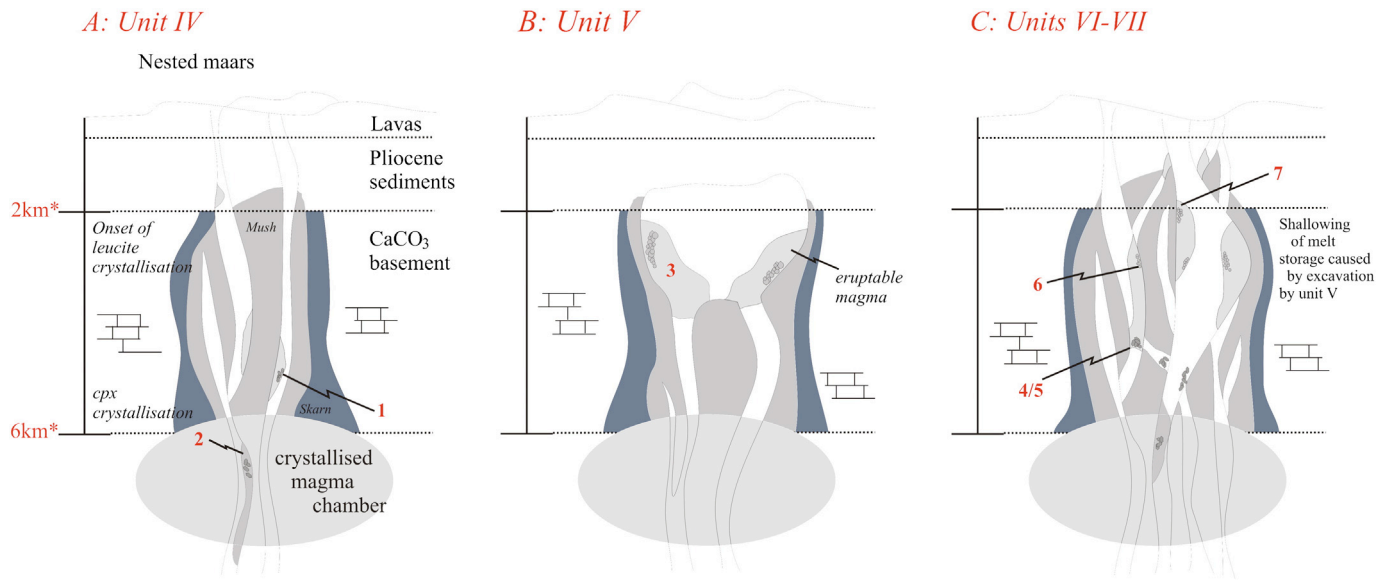


**Fig. 10.** Schematic drawing that illustrates a change in the Albano Maar magmatic system through time, based upon evidence from the pumice clasts. (A) Unit IV, (B) Unit V (Peperino ignimbrite) and (C) Units VI and VII.

reservoir (Giordano et al., 2002). It is therefore surprising that tephra associated with this eruption has not been found in the LGdM core. This may suggest that the dispersal axis was not to the SSE, as previously suggested (Giaccio et al., 2007, 2009).

Only one juvenile pumice clast type has been found within the deposits and they are heavily vesiculated (Fig. 3). The melt chemistry and texture of this clast type indicate that the magma underwent pre-eruptive leucite crystallisation after contamination with  $\text{CaCO}_3$  (Fig. 6). Recent work by Shea et al. (2009) has determined two models for natural crystallisation conditions that are consistent with their experimental data (1) leucite forms at ~4 km depth ( $P \sim 100$  MPa) in a magma saturated with  $\text{H}_2\text{O}$  or, (2) the magma was initially undersaturated with respect to  $\text{H}_2\text{O}$  and the leucite forms during slow depressurisation. This understanding alongside work completed by Vinkler et al. (2012) suggests that the increase in syn-eruptive crystallisation of leucite (apparent in the clasts of the units that bracket Unit V) is caused by a decrease in  $\text{H}_2\text{O}$  saturation. This evidence indicates that these different clast groups must have been stored under variable conditions in terms of pressure, temperature and volatile content. The decrease in  $\text{H}_2\text{O}$  saturation of the melt was potentially caused by an influx of  $\text{CO}_2$  from a Ca-rich melt (or similar shallow contaminator). This also highlights the key differences between clasts from Unit V (Peperino ignimbrite) and the eruptions that bracket it (Units IV, VI and VII). We can propose that syn-eruptive magma of Unit V were  $\text{H}_2\text{O}$  saturated and stored under steady-state magmatic conditions, prior to degassing and eruption, whereas the other units were  $\text{H}_2\text{O}$  undersaturated.

The larger proportions of lithics found in Unit V indicate excavation and entrainment of a larger volume of the crust (xenolith content = ~30%vol, Fig. 2) as an integral part of the explosive eruption. During the proposed longer residence, the magma could have been subject to repeated input of Ca-rich melt and  $\text{CO}_2$  over time until a critical saturation level was reached to trigger eruption. Unfortunately, it is not possible to determine the extent of Ca-rich melt contamination in this sample due to the effect of leucite crystallisation on the glass chemistry. However the high degree of vesiculation and the lithic contents of the deposit, reflecting excavation of a depth range down to ~6 km in a diatreme-style eruption, indicate that  $\text{CO}_2/\text{H}_2\text{O}$  variations in the magma probably triggered the eruption, rather than interaction with groundwater, suggesting it was magmatic rather than phreatomagmatic.

### 6.3.3. Unit VI (ca. 35 ka)

The age of Unit VI is inferred from the proximal–distal correlation with TM-17bc, and this implies a repose period of 1 ka between the Unit V (Peperino ignimbrite) and Unit VI eruptions. It could be suggested that there was shallowing of magma storage into the carbonate pre-volcanic basement (1–6 km) after the large excavating eruption of Unit V (Peperino ignimbrite; Fig. 10C). After this eruption, eruptive style reverted to melt-rich ballistic and fall with a much smaller deposit volume. The shallowing of storage and small melt volume of Unit VI helps to explain why this glass (melt) is the most contaminated (by Ca-rich melt) of the foiditic melt compositions analysed (Fig. 8C–E). Furthermore, it is the only unit that has been recorded in LGdM (TM-17bc). This dispersal may be due to SSE dispersion axis or to greater explosivity, a result of the larger volatile input caused by increased interaction with the Ca-rich melt leading to volatile release. The melt composition indicates that contamination occurred late stage, thus causing it to be volatile-charged and explosive.

### 6.3.4. Unit VII (ca. 3 ka)

The same process is recorded in the melt chemistry of Unit VII as in Unit VI. However, Unit VII has a fall and flow eruptive style and higher melt and lower lithic content (juvenile clasts = 90%; Fig. 8A) than Unit VI. The glass compositions in this unit are highly variable (Table 1) and record storage at three stratigraphic levels in the magma plumbing system, suggesting that multiple magma batches existed prior to eruption as shown in Fig. 10C. The deposit is also less fragmented than other Albano Maar units, being the only unit with a pumice-rich layer in the stratigraphy (Fig. 2). The predominance of syn-eruptive crystallisation of leucite in all of the three magma components is suggestive of a decrease in  $\text{XH}_2\text{O}$  in the magma allowing for crystallisation on ascent (Shea et al., 2009). This could either be caused by a change in late stage contamination by the surrounding wall rock or a difference in the primary magma composition.

## 7. Summary and conclusions

The main conclusions that can be drawn from this study are:

- 1) Albano maar is an unusual polygenetic maar complex, formed by seven, small volume explosive eruptions, of low viscosity, foiditic melt and phonolitic melt between ca 69 and 33 ka

- 2) The shallow crustal structure (carbonate at 1–6 km) is pivotal in defining two different magmatic evolutionary paths during high level magma storage in the small magmatic reservoirs of the Albano maar. Phono-tephritic magmas contaminated with carbonate evolve towards K-foidite (Path 1) whereas an absence of interaction with carbonate contamination allows evolution towards a more silica saturated phonolite (Path 2). Glass chemistry reveals a predominance of magmatic evolution via Path 1 to K-foidites (i.e. carbonate contamination)
- 3) A Ca-rich melt, generated by interaction with shallow pre-volcanic carbonate basement accounts for most of the foiditic melts recording a late stage, post-crystallisation mixing event (up to 50% mixing)
- 4) CaCO<sub>3</sub> contamination was persistent throughout high level crystallisation to allow for evolution from relatively unfractionated (primitive) phonolitic tephrite towards K-foidite and for late stage, post crystallisation contamination with CaCO<sub>3</sub>
- 5) Significant input of volatile CO<sub>2</sub> to the magma resulted from mixing with a Ca-rich melt, provides an alternative high level trigger for the explosivity of the silica-undersaturated system. According to this interpretation the Albano Maar would be considered a shallow diatreme, associated with the release of CO<sub>2</sub>, similar to a kimberlite pipe, rather than a typical phreatomagmatic maar
- 6) Volumetrically small and irregular melt volumes (i.e. larger surface area) enhances interaction and assimilation with carbonate basement (>Ca-rich melt:silicate melt) evident as a temporal increase in explosivity and dispersal (correlation of Unit VI to distal layer TM-17bc, 300 km SSE in LGdM)
- 7) Peperino ignimbrite (Unit V) resided in the shallow crust prior to eruption allowing for significant pre-degassing crystallisation of leucite. This implies storage under steady state magma chamber conditions and potentially longer residence time than that of other Albano Maar magmas.
- 8) Multiple regions of magma storage within the shallow crust (<6 km depth) can be constrained from variation in juvenile clast type and texture between, and within, different eruptions.
- 9) A large output of CO<sub>2</sub> prior to, and during, explosive eruptions at Albano Maar can be inferred from the unusual late stage contamination of magmas. This may in part account for current CO<sub>2</sub> emissions (ca. ~0.7 kg m<sup>-2</sup> day<sup>-1</sup>) (Chiodini and Frondini, 2001)
- 10) Should a new magma batch rise at shallow crustal levels (~6 km), the potential for explosive interaction with carbonates may trigger a significant volcanic hazard in the future.

## Acknowledgments

We acknowledge the NERC grant NE/E015905/1. NERC RESET Consortium publication number RHOX/030. We also thank Carmela Freda for a detailed review that improved the quality of this manuscript.

## Appendix A. Supplementary data

Supplementary data to this article can be found online at <http://dx.doi.org/10.1016/j.lithos.2013.11.001>.

## References

- Anzidei, M., Carapezza, M.L., Esposito, A., Giordano, G., Tarchini, L., Lelli, M., 2008. The Albano Maar Lake High resolution bathymetry and dissolved CO<sub>2</sub> budget (Colli Albani District, Italy): constraints to hazard evaluation. *Journal of Volcanology and Geothermal Research* 171, 258–268.
- Avanzinelli, R., Elliott, T., Tommasini, S., Conticelli, S., 2008. Constraints on the genesis of the potassium-rich Italian volcanics from U/Th disequilibrium. *Journal of Petrology* 49, 195–223.
- Avanzinelli, R., Lustrino, M., Mattei, M., Melluso, L., Conticelli, S., 2009. Potassic and ultrapotassic magmatism in the circum-Tyrrhenian region: significance of carbonated pelitic vs. pelitic sediment recycling at destructive plate margins. *Lithos* 113 (1–2), 213–227.
- Behrens, H., Misiti, V., Freda, C., Vetere, F., Botcharnikov, R., Scarlato, P., 2009. Solubility of H<sub>2</sub>O and CO<sub>2</sub> in ultrapotassic melts at 1200 and 1250 °C and pressure from 50 to 500 MPa. *American Mineralogist* 94, 105–120.
- Bianchi, L., Piana Agostinetti, N., De Gori, P., Chiarabba, C., 2008. Deep structure of the Colli Albani volcanic district (Central Italy) from receiver functions analysis. *Journal of Geophysical Research* 113 (B9), 2156–2202.
- Blundy, J., Cashman, K., 2001. Ascent driven crystallisation of dacite magmas at Mount St Helens, 1980–1986. *Contributions to Mineralogy and Petrology* 140 (6), 631–650.
- Boari, E., Avanzinelli, R., Melluso, L., Giordano, G., Mattei, M., De Benedetti, A.A., Morra, V., Conticelli, S., 2009. Isotope geochemistry (Sr–Nd–Pb) and petrogenesis of leucite-rich volcanic rocks from “Colli Albani” volcano, Roman Comagmatic Province, Central Italy: inferences on volcano evolution and magma genesis. *Bulletin of Volcanology* 71 (9), 977–1005.
- Botcharnikov, R.E., Behrens, H., Holtz, F., 2006. Solubility and speciation of C–O–H fluids in andesitic melt at T = 1100–1300 °C and P = 200 and 500 MPa. *Chemical Geology* 229, 125–143.
- Brooker, R.A., Hamilton, D.L., 1990. Three liquid immiscibility and the origin of carbonatites. *Nature* 346, 459–462.
- Brooker, R.A., Kjarsgaard, B.A., 2011. Silicate carbonate liquid immiscibility and phase relations in the system SiO<sub>2</sub>–Na<sub>2</sub>O–Al<sub>2</sub>O<sub>3</sub>–CaO–CO<sub>2</sub> at 0.1–2.5 GPa with applications to carbonatite genesis. *Journal of Petrology* 52 (7–8), 1281–1305.
- Büttner, R., Dellino, P., Zimanowski, B., 1999. Identifying magma–water interaction from surface features of ash particles. *Nature* 401, 688–690.
- Carapezza, M.L., Tarchini, L., 2007. Accidental gas emission from shallow pressurized aquifers at Alban Hills volcano (Rome, Italy): geochemical evidence of magmatic degassing? *Journal of Volcanology and Geothermal Research* 165, 5–16.
- Chiarabba, C., Amato, A., Delaney, P.T., 1997. Crustal structure, evolution and volcanic unrest at Alban Hills, central Italy. *Bulletin of Volcanology* 59, 161–170.
- Chiarabba, C., Giordano, G., Mattei, M., Funicello, R., 2010. The three-dimensional structure of the Colli Albani volcano. In: Funicello, R., Giordano, G. (Eds.), *The Colli Albani Volcano*. Special Publication of IAVCEI. The Geological Society of London, pp. 29–42.
- Chiodini, G., Frondini, F., 2001. Carbon dioxide degassing from the Alban Hills volcanic region, central Italy. *Chemical Geology* 177, 67–83.
- Conticelli, S., Boari, E., Avanzinelli, R., De Benedetti, A.A., Giordano, G., Mattei, M., Melluso, M., Morra, V., 2010. Geochemistry, isotopes and mineral chemistry of the Colli Albani volcanic rocks: constraints on magma genesis and evolution. In: Funicello, R., Giordano, G. (Eds.), *The Colli Albani Volcano*. Special Publication of IAVCEI. The Geological Society of London, pp. 107–140.
- Cross, J.K., Roberge, J., Jerram, D.A., 2012. Constraining the degassing processes of Popocatepetl Volcano, Mexico: a vesicle size distribution and glass geochemistry study. *Journal of Volcanology and Geothermal Research* 225–226, 81–95.
- D’Orazio, M., Innocenti, F., Tonarini, S., Dogliani, C., 2007. Carbonatites in a subduction system: the Pleistocene alvikites from Mt. Vulture (southern Italy). *Lithos* 98, 313–334.
- Danese, E., Mattei, M., 2010. The sedimentary substrate of the Colli Albani. In: Funicello, R., Giordano, G. (Eds.), *The Colli Albani Volcano*. Special Publication of IAVCEI. The Geological Society of London, pp. 141–152.
- De Benedetti, A.A., Funicello, R., Giordano, G., Diano, G., Caprilli, E., Paterne, M., 2008. Volcanology, history and myths of the lake Albano maar (Colli Albani volcano, Italy). *Journal of Volcanology and Geothermal Research* 176, 387–406.
- De Benedetti, A.A., Caprilli, E., Rossetti, F., Giordano, G., 2010. Metamorphic, metasomatic and intrusive xenoliths of the Colli Albani volcano and their significance for the reconstruction of the volcano plumbing system. In: Funicello, R., Giordano, G. (Eds.), *The Colli Albani Volcano*. Special Publication of IAVCEI. The Geological Society of London, pp. 153–176.
- De Rita, D., Faccenna, C., Funicello, R., Rosa, C., 1995. Stratigraphy. In: Trigila, R. (Ed.), *The Volcano of the Alban Hills*. Tipografia SGS, Rome, pp. 33–73.
- Deegan, F.M., Troll, V.R., Freda, C., Misiti, V., Chadwick, J.P., McLeod, C., Davidson, J.P., 2010. Magma–carbonate interaction processes and associated CO<sub>2</sub> release at Merapi Volcano, Indonesia: insights from experimental petrology. *Journal of Petrology* 51 (5), 1027–1051.
- Di Rocco, T., Freda, C., Gaeta, M., Mollo, S., Dallai, L., 2012. Magma chambers emplaced in carbonate substrate: petrogenesis of skarn and cumulate rocks and implications for CO<sub>2</sub> degassing in volcanic areas. *Journal of Petrology* 53 (11), 2307–2332.
- Freda, C., Gaeta, M., Karner, D.B., Marra, F., Renne, P.R., Taddeucci, J., Scarlato, P., Christensen, J.N., Dallai, L., 2006. Eruptive history and petrologic evolution of the Albano multiple maar (Alban Hills, Central Italy). *Bulletin of Volcanology* 68, 567–591.
- Freda, C., Gaeta, M., Misiti, V., Mollo, S., Dolfi, D., Scarlato, P., 2008. Magma–carbonate interaction: an experimental study on ultrapotassic rocks from Alban Hills (Central Italy). *Lithos* 101, 397–415.
- Freda, C., Gaeta, M., Giaccio, B., Marra, F., Palladino, D.M., Scarlato, P., Sotilli, G., 2011. CO<sub>2</sub>-driven large mafic explosive eruptions: the Pozzolane Rosse case study from the Colli Albani Volcanic District (Italy). *Bulletin of Volcanology* 73 (3), 241–256.
- Funicello, R., Giordano, G., De Rita, D., 2003. The Albano Maar lake (Colli Albani volcano, Italy): recent volcanic activity and evidence of pre-Roman Age catastrophic lahar events. *Journal of Volcanology and Geothermal Research* 123, 43–61.
- Gaeta, M., Freda, C., Christensen, J.N., Dallai, L., Marra, F., Karner, D.B., Scarlato, P., 2006. Time-dependent geochemistry of clinopyroxene from the Alban Hills (Central Italy): clues to the source and evolution of ultrapotassic magmas. *Lithos* 86, 330–346.
- Gaeta, M., Di Rocco, T., Freda, C., 2009. Carbonate assimilation in open magmatic systems: the role of melt-bearing skarns and cumulate-forming processes. *Journal of Petrology* 50 (2), 361–385.

- Gaeta, M., Freda, C., Marra, F., Di Rocco, T., Gozzi, F., Arienzo, I., Giaccio, B., Scarlato, P., 2011. Petrology of the most recent ultrapotassic magmas from the Roman Province (Central Italy). *Lithos* 127 (1–2), 298–308.
- Giaccio, B., Sposato, A., Gaeta, M., Marra, F., Palladino, D.M., Taddeucci, J., Barbieri, M., Messini, P., Rolfo, M.F., 2007. Mid-distal occurrences of the Albano Maar pyroclastic deposits and their relevance for reassessing the eruptive scenarios of the most recent activity at the Colli Albani Volcanic District, Central Italy. *Quaternary International* 171–172, 160–178.
- Giaccio, B., Marra, F., Hajdas, I., Karner, D.B., Renne, P.R., Sposato, A., 2009.  $^{40}\text{Ar}/^{39}\text{Ar}$  and  $^{14}\text{C}$  geochronology of the Albano maar deposits: implications for defining the age and eruptive style of the most recent explosive activity at Colli Albani Volcanic District, Central Italy. *Journal of Volcanology and Geothermal Research* 185, 203–213.
- Giordano, G., CARG Team, 2010. Stratigraphy, volcano tectonics and evolution of the Colli Albani field. In: Funicello, R., Giordano, G. (Eds.), *The Colli Albani Volcano*. Special Publication of IAVCEI. The Geological Society of London, pp. 43–98.
- Giordano, G., De Rita, D., Cas, R., Rodani, S., 2002. Valley pond and ignimbrite veneer deposits in the small-volume phreatomagmatic 'Peperino Albano' basic ignimbrite, Lago Albano maar, Colli Albani volcano, Italy: influence of topography. *Journal of Volcanology and Geothermal Research* 118, 113–144.
- Giordano, G., De Benedetti, A.A., Diana, A., Diano, G., Gaudio, F., Marasco, F., Miceli, M., Mollo, S., Cas, R.A.F., Funicello, R., 2006. The Colli Albani mafic caldera (Roma, Italy): stratigraphy, structure and petrology. *Journal of Volcanology and Geothermal Research* 155, 49–80.
- Iacono Marziano, G., Gaillard, F., Pichavant, M., 2007. Limestone assimilation and the origin of  $\text{CO}_2$  emissions at the Alban Hills (Central Italy): constraints from experimental petrology. *Journal of Volcanology and Geothermal Research* 166, 91–105.
- Iacono Marziano, G., Gaillard, F., Pichavant, M., 2008. Limestone assimilation by basaltic magmas: an experimental re-assessment and application to Italian volcanoes. *Contributions to Mineralogy and Petrology* 155, 719–738.
- Iacono Marziano, G., Paonita, A., Rizzo, A., Scaillet, B., Gaillard, F., 2010. Noble gas solubilities in silicate melts: new experimental results and a comprehensive model of the effects of liquid composition, temperature and pressure. *Chemical Geology* 279 (3–4), 145–157.
- Jambon, A., 1983. Diffusion dans les silicates fondus: Un bilan des connaissances actuelles. *Bull. Mineral.* 106, 229–246.
- Jochum, K.P., Stoll, B., Herwig, K., Willbold, M., Hofmann, A.W., Amini, M., Aarburg, S., Abouchami, W., Hellebrand, E., Mocek, B., Raczek, I., Stracke, A., Alard, O., Bouman, C., Becker, S., Dücking, M., Brätz, H., Klemd, R., De Bruin, D., Canil, D., Cornel, I. D., De Hoog, J.C.M., Dalpé, C., Danyushevsky, L.V., Eisenhauer, A., Gao, Y., Snow, J.E., Groschopf, N., Günther, D., Latkoczy, C., Guillong, M., Hauri, E., Höfer, H.E., Lahaye, Y., Horz, K., Jacob, D.E., Kasemann, S., Kent, A.J.R., Zack, T., Ludwig, T., Mason, P.R.D., Meixner, A., Rosner, M., Misawa, K., Nash, B.P., Pfänder, J.A., Premo, W.R., Sun Weidong, D., Tiepolo, M., Vannucci, R., Vennemann, T., Wayne, D., Woodhead, J.D., 2006. MPI-DING reference glasses for in situ microanalysis: new reference values for element concentrations and isotope ratios. *Geochemistry, Geophysics, Geosystems* 7, Q02008 (GeoReM 658).
- Karner, D.B., Marra, F., Renne, P.R., 2001. The history of the Monti Sabatini and Alban Hills volcanoes: groundwork for assessing volcanic–tectonic hazards for Rome. 107 (1–3), 185–215.
- Langmuir, C.H., Vocke, R.D., Hanson, G.N., 1978. A general mixing equation with applications to Icelandic basalts. *Earth and Planetary Science Letters* 37, 380–392.
- Lorenz, V., 1986. On the growth of maars and diatremes and its relevance to the formation of tuff rings. *Bulletin of Volcanology* 48, 265–274.
- Lowenstern, J.B., 2001. Carbon dioxide in magmas and implications for hydrothermal systems. *Mineralium Deposita* 36, 490–502.
- Marra, F., Freda, C., Scarlato, P., Taddeucci, J., Karner, D.B., Renne, P.R., Gaeta, M., Palladino, D.M., Trigila, R., Cavarretta, G., 2003. Post-caldera activity in the Alban Hills volcanic district (Italy):  $^{40}\text{Ar}/^{39}\text{Ar}$  geochronology and insights into magma evolution. *Bulletin of Volcanology* 65, 227–247.
- Martelli, M., Nuccio, P.M., Stuart, F.M., Burgess, R., Ellam, R.M., Italiano, F., 2004. Helium–strontium isotope constraints on mantle evolution beneath the Roman Comagmatic Province, Italy. *Earth and Planetary Science Letters* 224, 295–308.
- Melzer, S., Foley, S.F., 2000. Phase relations and fractionation sequences in potassium series modelled in the system  $\text{CaMgSiO}_2\text{--KAlSiO}_4\text{--MgSiO}_4\text{--SiO}_2\text{--F}_2\text{O}_1$  at 1 bar to 18 kbar. *Contributions to Mineralogy and Petrology* 138 (2), 186–197.
- Mollel, G.F., Swisher, C.C., 2011. The Ngorongoro Volcanic Highland and its relationships to volcanic deposits at Olduvai Gorge and East African Rift volcanism. *Journal of Human Evolution* 63 (2), 274–283.
- Mollo, S., Gaeta, M., Freda, C., Di Rocco, T., Misiti, V., Scarlato, P., 2010. Carbonate assimilation in magmas: a reappraisal based on experimental petrology. *Lithos* 114, 503–514.
- Müller, W., Shelley, M., Miller, P., Broude, S., 2009. Initial performance metrics of a new custom-designed ArF excimer LA-ICP-MS system coupled to a two-volume laser ablation cell. *Journal of Analytical Atomic Spectrometry* 24, 209–214.
- Palladino, D.M., Gaeta, M., Marra, F., 2001. A large foiditic hydromagmatic eruption from the early activity of the Alban Hills Volcanic District, Italy. *Bulletin of Volcanology* 63, 345–359.
- Pardo, N., Macias, J.L., Giordano, G., Cianfarra, P., Bellatreccia, F., Avellán, D.R., 2009. The 1245 yr BP Asososca maar eruption: the youngest event along the Nejapa-Miraflores volcanic fault, western Managua, Nicaragua. *Journal of Volcanology and Geothermal Research* 184 (3–4), 292–312.
- Peccerillo, A., 2005. Plio-Quaternary volcanism in Italy. *Petrology, Geochemistry, Geodynamics*. Springer, Heidelberg, 365 pp.
- Porreca, M., Mattei, M., MacNiocaill, C., Giordano, G., McClelland, E., Funicello, R., 2008. Paleomagnetic evidence for low-temperature emplacement of the phreatomagmatic Peperino Albano ignimbrite (Colli Albani volcano, Central Italy). *Bulletin of Volcanology* 70 (7), 877–893.
- Rosenbaum, G., Lister, G.S., 2004. Neogene and Quaternary rollback evolution of the Tyrrhenian Sea, the Apennines, and the Sicilian Maghrebides. *Tectonics* 23.
- Russell, J.K., Porritt, L.A., Lavallee, Y., Dingwell, D.B., 2012. Kimberlite ascent by assimilation-fuelled buoyancy. *Nature* 481 (19), 352–356.
- Shane, P., Smith, V.C., Nairn, I., 2008. Millennial timescale resolution of rhyolite magma recharge at Tarawera volcano: insights from quartz chemistry and melt inclusions. *Contributions to Mineralogy and Petrology* 156, 397–411.
- Shaw, C.S.J. and Woodland, A.B., 2012. The role of magma mixing in the petrogenesis of mafic alkaline lavas, Rockeskyllerkopf Volcanic Complex, West Eifel, Germany. 74, 359–376.
- Shea, T., Larsen, J.F., Gurioli, L., Hammer, J.E., Houghton, B.F., Cioni, R., 2009. Leucite crystals: surviving witnesses of magmatic processes preceding the 79 AD eruption at Vesuvius, Italy. *Earth and Planetary Science Letters* 281, 88–98.
- Sottili, G., Taddeucci, J., Palladino, D.M., Gaeta, M., Scarlato, P., Ventura, G., 2008. Sub-surface dynamics and eruptive styles of maars in the Colli Albani Volcanic District, Central Italy. *Journal of Volcanology and Geothermal Research* 180, 189–202.
- Sun, S.S., McDonough, W.F., 1989. Chemical and isotopic systematics of oceanic basalts: implications for mantle composition and processes. In: Saunders, A.D., Norry, M.J. (Eds.), *Magmatism in the Ocean Basins*. Geological Society Special Publication, 42, pp. 313–345.
- Tomlinson, E.L., Thordason, T., Müller, W., Thirwall, M., Menzies, M.A., 2010. Micro-analysis of tephra by LA-ICP-MS—strategies, advantages and limitations assessed using the Thorsmörk ignimbrite (Southern Iceland). *Chemical Geology* 279 (3–4), 73–89.
- Trigila, R., Agosta, E., Currado, C., De Benedetti, A.A., Freda, C., Gaeta, M., Palladino, D.M., Rosa, C., 1995. Petrology. In: Trigila, R. (Ed.), *The Volcano of the Alban Hills*. Tipografia SGS, Rome, pp. 95–165.
- Vinkler, A.P., Cashman, K., Giordano, G., Groppelli, G., 2012. Evolution of the mafic Villa Senni caldera-forming eruption at Colli Albani volcano, Italy, indicated by textural analysis of juvenile fragments. *Journal of Volcanology and Geothermal Research* 235–236, 37–54.
- Wohletz, K.H., 1986. Explosive magma–water interactions: thermodynamics, explosion mechanisms, and field studies. *Bulletin of Volcanology* 48 (5), 245–264.
- Wulf, S., Keller, J., Paterne, P., Mingram, J., Lauterbach, S., Opitz, S., Sottili, G., Giaccio, B., Albert, P.G., Satow, C., Tomlinson, E.L., Viccaro, M., Brauer, A., 2012. The 100–133 ka record of Italian explosive volcanism and revised tephrochronology of Lago Grande di Monticchio. *Quaternary Science Reviews* 58, 104–123.